J Neurophysiol 115: 773–789, 2016.
First published November 18, 2015; doi:10.1152/jn.00695.2015.

The rostral ventromedial medulla control of cutaneous vasomotion of paws and tail in the rat: implication for pain studies

Nabil El Bitar,[1,2]* Bernard Pollin,[1,2]*† Gan Huang,[3] André Mouraux,[3] and Daniel Le Bars[1,2]
[1]*Sorbonne Universités, Université Pierre et Marie Curie, Faculté de Médecine, Paris, France;* [2]*Neurosciences Paris-Seine, Institut National de la Santé et de la Recherche Médicale UMRS-1130, Centre National de la Recherche Scientifique UMR-8246, Paris, France; and* [3]*Institute of Neuroscience, Université Catholique de Louvain, Brussels, Belgium*

Submitted 15 July 2015; accepted in final form 13 October 2015

El Bitar N, Pollin B, Huang G, Mouraux A, Le Bars D. The rostral ventromedial medulla control of cutaneous vasomotion of paws and tail in the rat: implication for pain studies. *J Neurophysiol* 115: 773–789, 2016. First published November 18, 2015; doi:10.1152/jn.00695.2015.— Thermal neutrality in rodents is achieved by large cyclic variations of the sympathetic drive of the vasomotion of the tail and paws, the most widely used target organs in current acute or chronic animal models of pain. Given the pivotal functional role of rostral ventromedial medulla (RVM) in nociception and rostral medullary raphe (rMR) in thermoregulation, two largely overlapping brain regions, we aimed at circumscribing the brainstem regions that are the source of premotor afferents to sympathetic preganglionic neurons that control the vasomotor tone of the tail and hind paws. A thermometric infrared camera recorded indirectly the vasomotor tone of the tail and hind paws. During the control period, the rat was maintained in vasoconstriction by preserving a stable, homogeneous, and constant surrounding temperature, slightly below the core temperature. The functional blockade of the RVM/rMR by the $GABA_A$ receptor agonist muscimol (0.5 nmol, 50 nl) elicited an extensive increase of the temperature of the paws and tail, associated with a slight decrease of blood pressure and heart rate. Both the increased heat loss through vasodilatation and the decrease heart-induced heat production elicited a remarkable reduction of the central temperature. The effective zones were circumscribed to the parts of the RVM/rMR facing the facial nucleus. They match very exactly the brain regions often described as specifically devoted to the control of nociception. Our data support and urge on the highest cautiousness regarding the interpretation of results aimed at studying the effects of any pharmacological manipulations of RVM/rMR with the usual tests of pain.

rat; thermoregulation; ambient temperature; skin temperature; environmental impact; blood pressure; heart rate; infrared camera; rostral ventromedial medulla; RVM; rostral medullary raphe; rMR

NUMEROUS STUDIES HAVE EXPLORED the descending systems that control the spinal transmission of nociceptive messages, notably through the rostral ventromedial medulla (RVM) in the brainstem. The RVM includes the nucleus raphe magnus and the neighboring part of the reticular formation, which extends under the gigantocellular reticular nucleus (Fields et al. 2006). Two main categories of neurons, so-called "on-" and "off-" cells, were highlighted that *1*) exhibit irregular spontaneous activities in opposition of phase (Barbaro et al. 1989) and *2*) are activated and inhibited by nociceptive stimuli, respectively (Fields et al. 1983; Vanegas et al. 1984). These two neuronal types were proposed to belong to a double spino-bulbo-spinal positive feedback loop that facilitates the spinal transmission of nociceptive messages, either directly or through a mechanism of disinhibition, the on- and off-cells being supposed to produce an excitatory and an inhibitory drive on the spinal neurons, respectively.

However, RVM neurons could play a much less specific role than that of a descending pathway modulating nociception at spinal level (Le Bars et al. 2001; Lefler et al. 2008; Lovick 1997; Mason 2001, 2005a,b, 2006, 2011, 2012; Thurston and Helton 1996; Thurston and Randich 1992, 1995). For example, we described recently the probable involvement of on- and off-cells in autonomic regulation, notably thermoregulation (El Bitar et al. 2014b).

On the basis of three animal models used in thermoregulation studies, namely the tail of the rat, the ear of the rabbit, and the interscapular brown adipose tissue (BAT) of the rat, it became apparent that neurons in the midline region of the ventral medulla play a critical role in responding to cold (Blessing et al. 1999; McAllen et al. 2010; Morrison 1999, 2011; Morrison et al. 1999, 2008, 2012; Nakamura 2011; Nakamura and Morrison 2008, 2011; Rathner et al. 2001; Rathner and McAllen 1999; Tanaka et al. 2002). Broadly, cooling the animal results in *1*) reduced heat loss through increased skin vasoconstriction of the ear in the rabbit or the tail in the rat and *2*) increased heat production by BAT in the rat. These phenomena are triggered by activation of sympathetic preganglionic neurons in the spinal intermediolateral cell column, themselves under the control of premotor neurons located in the rostral medullary raphe (rMR), a region immediately rostral to the rostral pole of the inferior olivary complex, that includes the raphe pallidus, the raphe magnus, and the laterally extending parapyramidal nucleus (Blessing 2003; McAllen et al. 2010; Morrison 2011; Nakamura 2011; Nakamura and Morrison 2008, 2011), where the expression of Fos immunoreactivity is increased following cold exposure (Bonaz and Taché 1994; Cano et al. 2003; Morrison et al. 1999; Nakamura et al. 2004).

Yet a possible discrepancy was noted. Studies focusing on the descending systems postulated to control nociception emphasize a region that includes the nucleus raphe magnus and the gigantocellular reticular nucleus pars alpha, mainly at the level of the facial nucleus (e.g., Brink et al. 2006; Carlson et al. 2007; Fields et al. 1995; Heinricher and Kaplan 1991; Heinricher and Tortorici 1994; Kaplan and Fields 1991; Morgan and Fields 1994; Neubert et al. 2004; Vanegas et al. 1984; Thurston and Helton 1996; Thurston and Randich 1995; Xu et al. 2007), while studies focusing on thermoregulation empha-

* N. El Bitar and B. Pollin contributed equally to this work.
† Deceased 26 March 2015.
Address for reprint requests and other correspondence: D. Le Bars, Sorbonne Universités, Université Pierre et Marie Curie, Faculté de Médecine Paris, France (e-mail: daniel.le_bars@upmc.fr).

size a slightly more caudal region including the raphe pallidus (e.g., Blessing and Nalivaiko, 2001; Cao and Morrison 2003; Cao et al. 2004, 2010; Cerri et al. 2010; Fan et al. 2007; Madden and Morrison 2003, 2005; Morrison 1999, 2003, 2004; Morrison et al. 1999, 2000; Nakamura and Morrison 2007, 2011; Nakamura et al. 2004; Ootsuka and McAllen 2005; Rathner et al. 2001, 2008; Salo et al. 2009; Tanaka et al. 2002, 2007; Yoshida et al. 2003).

The aim of the present study was therefore to exactly map the brainstem regions that contain the premotor sympathetic neurons controlling the vasomotor tone of the tail and hind paws of the rat and to compare these locations with that of nociception-related brainstem areas. This choice was made specifically because many behavioral models of pain/nociception are based on the assessment of the response of a rodent to a thermal stimulus applied to the tail or a hind paw (reviewed in Le Bars et al. 2001, 2009).

Specifically, we measured in 160 adult male Sprague-Dawley rats the dynamic changes in vasomotor tone induced by microinjections of muscimol within these regions. During the injection, the rats were maintained in a stable state of tail and hind paw vasoconstriction. Microinjection of muscimol within the RVM/rMR was expected to elicit vasodilation of the tail and hind paw. When a vasomotor response was present, the latency at which vasodilation occurred was used as an index of the distance between the injection site and the structure generating the response.

Glossary

α	Slope of the squared temperature variation elicited by a radiant heat source ($°C^2/s$)
bpm	Beats per minute
Δt	Duration of the ascending phases of vasodilatation ($= t_{max} - t_{min}$)
paw-contra	Mid-plantar area on the hind paw, contralateral to the injection site
paw-ipsi	Mid-plantar area on the hind paw, ipsilateral to the injection site
t_{min}	Beginning time of the ascending phase of vasodilatation (min)
t_{max}	End time of the ascending phase of vasodilatation (min)
t_x	Abscissa of the inflection point of Boltzmann sigmoid (min)
T_{adj}	Sigmoid Boltzmann curve adjusted to the recorded temperature
T_{max}	Adjusted maximal skin temperature at the end of the process of vasodilatation (°C)
T_{min}	Adjusted skin temperature during the control period (°C)
T_{skin}	Temperature of the skin (°C)
T_x	Ordinate of the inflection point of Boltzmann sigmoid (°C)
x	Latero-lateral coordinate with reference to the interaural line
y	Ventrodorsal coordinate with reference to the interaural line
z	Rostrocaudal coordinate with reference to the interaural line

METHODS

Ethic statement. Animal experiments were performed with permission of the Board of the Veterinarian Services of the French Ministry of Agriculture (Permit No. 75–151) in accordance with the National Institutes of Health *Guide for the Care and Use of Laboratory Animals*, the European Communities Council Directive 86/609/EEC regulating animal research, and the Ethics Committee of the International Association for the Study of Pain (Covino et al. 1980; Zimmermann 1983). The Ethics Committee in Animal Experiment Charles Darwin approved the procedures.

Animals. Experiments were performed on 160 adult male Sprague-Dawley rats (Janvier Labs, Saint-Berthevin, France) weighing 320–370 g. They were housed in groups of three to four per cage, allowed free access to food and water with a 12-h alternating light-dark cycle, and acclimatized to the laboratory for at least 1 wk before the experiment. The experiments were conducted between 9 AM and 5 PM.

Experimental procedure. The animals were deeply anesthetized with 2.5% halothane in 100% oxygen. A tracheal cannula was inserted and the ventilation was controlled mechanically with an open circuit respirator equipped with a scavenging system, at a rate of 50 breaths/min. The tidal volume was adjusted to maintain a normal end-tidal CO_2 ($ETCO_2$). The expiratory halothane level and $ETCO_2$ were assessed with a capnometer (Capnomac II, Datex Instruments, Helsinki, Finland), recorded each 10 s and under control of alarms throughout the experiment. The mean arterial blood pressure (MAP) and heart rate (HR) were monitored continuously via a catheter inserted into the common carotid artery and connected to a computer via a transducer. MAP and HR were calculated and recorded using the NOTOCORD blood pressure analyzer system.

The body of the animal was wrapped up in a water-warming pad connected to an extra-capacity water circulator (TP 220-Kent; Scientific) sparing the head, the paws, and the tail. The heating blanket was covered with an isothermic metalized polyester film ("survival blanket") to stabilize the space temperature around the body. A two-channel OMEGA HH506RA digital thermometer and two VIP-T-CT25515 Probes (0.1°C resolution) were used to measure the core temperature T_{core} (throughout a rectal probe inserted 10 cm) and the heating temperature T_{warm} (probe placed between the warming pad and the trunk of the rat). We adjusted T_{warm} to maintain *1*) T_{core} stable within normal physiological values and *2*) the tail and hind paws in vasoconstriction.

The rat was mounted on a Horsley-Clarke stereotaxic frame. The, 0.5 ml of xylocaine 2% was injected subcutaneously in the scalp, followed by a 2-cm midline incision. After trepanation, a small incision of the dura mater was made to introduce the tip of a microinjection glass needle.

After surgery, halothane was decreased to 0.8–0.9% with oxygen being kept at 100%, the tidal volume was adjusted to keep the $ETCO_2$ around 3.5% and there was a wait of at least 30 min before the experimental procedure was started. After 15-min of control period in steady vasoconstriction, 57 ng (50 nl) muscimol were injected in the RVM/rMR (target zone between −0.8 and −3.3 rostral to interaural line) over 60 s. Since RVM and rMR largely overlap, we will refer to "RVM/rMR" for brain regions that include the raphe pallidus, raphe magnus, parapyramidal nucleus, and the reticular formation that extends under the gigantocellular reticular nucleus (Mason 2001, 2005a,b, 2006, 2011). Control experiments were conducted with the same procedure, except that muscimol was injected outside the RVM/rMR.

Experimental conditions. The experiments were made in anesthetized rat with unremitting halothane level [0.85 (0.83–0.86)%], while ventilation was controlled to achieve a stable and normal acid-base equilibrium during the control period $ETCO_2$ = 3.65 (3.57–3.73)%. The mean room temperature T_{amb} was stable at 24.2 (24.1–24.4)°C. The paws and tail of the rat were maintained in vasoconstriction

during the control period by preserving a stable, homogeneous and constant surrounding temperature [T_{warm} = 37.4 (37.2–37.5)°C], ≈ 0.3°C below T_{core} [37.7 (37.6–37.8)°C], and kept constant till the end of the experiment. In the control period, MAP and HR were 83.9 (77.4–90.4) mmHg and 321 (309–332) bpm, respectively.

Muscimol preparation. We prepared muscimol solution in a concentration of 0.01 nmol/nl, added pontamine sky blue to identify the site of injection, fractioned the solution in 2 μl aliquots for single use, and preserved them at −20°C. Muscimol produces a rapid and persistent hyperpolarization of neurons (Hikosaka and Wurtz 1985; Martin and Ghez 1999) based on its high affinity and selectivity for the $GABA_A$ receptor (Beaumont et al. 1978; Enna and Snyder 1975; Gallagher et al. 1983; Krogsgaard-Larsen et al. 1977; Nicholson et al. 1979). The day of the experiment, we filled the circuit of the glass needle with paraffin to wash out air bubbles, aspirated 0.5 μl of muscimol solution at the tip of the needle using a 1-μl Hamilton syringe, and introduced the needle in the brain at the end of the surgery.

Thermographic recordings. Under stable environmental temperature, skin temperature is a reliable indicator of skin blood flow variations (El Bitar et al. 2014a; Hertzman 1953). Heat transmission from deeper tissue to the skin occurs by conduction and vascular convection, and then heat dissipation to the environment occurs through conduction, convection, evaporation, and radiation processes. The spatial and temporal evolution of the skin temperature at the level of the tail and paws was monitored using a JADE MWIR (3- to 5-μm optical bandpass) camera (CEDIP Infrared Systems) with a 500-μs integration time, which supplied images of 320 × 240 pixels at 1 Hz with a sensitivity of 0.02°C at 25°C. The camera was placed 1.5 m upright to the scene and was controlled by the software Cirrus (CEDIP Infrared Systems). It was calibrated by means of a black body as previously described (Benoist et al. 2008).

Recently, we verified the highly significant positive linear correlation between skin temperature and skin blood flow measured by a laser-Doppler probe. The mean time lag between vasodilatation and skin temperature increase was estimated at around half a minute (El Bitar et al. 2014a). Such an approach based on thermal imaging has the advantage of giving accurate measures of temperature at both temporal and spatial levels.

Analysis of the thermographic films was made using the software Altair (CEDIP Infrared Systems, Croissy-Beaubourg, France). Ten regions of interest (ROIs) were defined in the recorded scene, each comprising 10 pixels. Five ROIs were located on the dorsal aspect of the tail. A proximal ROI (tail-prox) was placed 3 cm from the root of the tail, an intermediate ROI (tail-mid) was placed at the middle of the tail, and a distal ROI (tail-distal) was placed 3 cm from the tip of the tail. The remaining two zones were distributed equidistantly between tail-prox and tail-mid and tail-mid and tail-dist. Two additional ROIs were located on the plantar aspect of each hind paw; their final designation was defined respective to the side of muscimol microinjection, ipsilateral (paw-ipsi) or contralateral (paw-contra), as determined following histological controls. Finally, a ROI was located over a piece of wood placed in the scene to monitor the ambient temperature (T_{amb}). For each time point, the mean of the 10 pixels defining each ROI was computed to obtain one single temperature time course for each ROI ($T_{tail\text{-}prox}$, $T_{tail\text{-}mid}$, $T_{tail\text{-}dist}$, $T_{paw\text{-}left}$, $T_{paw\text{-}right}$, and T_{amb}).

Histological identification of microinjection sites. At the conclusion of the experiment, the rat was deeply anesthetized with 3% halothane and the brain was perfused through the heart with 0.9% NaCl, followed by 10% formaldehyde and removed. The brain was frozen, cut in serial 100-μm thick sections, and Nissl-stained with cresyl violet or carmin. Sites of microinjections were determined from microscopic visualization of the serial sections and reported on schemas of frontal sections of the brain (Paxinos and Watson 1986). Coordinates were then expressed relative to the interaural line: x-axis = latero-lateral; y-axis = ventrodorsal; and z-axis = rostrocaudal. The center of injection was easy to delimit. On average ~1 h postinjection, the overall rostrocaudal diffusion of pontamine blue was 1.1 (1.0–1.2) mm, that is two times longer than in the coronal plane.

Assessing the dynamic effects of muscimol on skin temperature. The skin temperature evolution following muscimol microinjection matched a sigmoid curve. The curves were adjusted to a Boltzmann sigmoid according to the equation $T_{adj} = T_{min} + \Delta T_{skin}/\{1 + \exp[-(t - t_x)/s]\}$, using the SigmaPlot software. Time $t = 0$ corresponded to the end of the microinjection (Fig. 1*A*). The following parameters were fitted to the data: T_{min} (adjusted skin temperature during the control period), T_{max} (adjusted maximal skin temperature at the end of the process), $\Delta T_{skin} = T_{max} - T_{min}$ (amplitude of the skin temperature variation), t_x (abscissa of the inflection point of the sigmoid), T_x (ordinate of the inflection point of the sigmoid), and s = spread of the sigmoid curve. These parameters were calculated for the proximal and distal parts of the tail and for each hind paw. The regression coefficients R^2 of the adjusted curves were always highly significant (>0.98).

The regulation of the laboratory air-conditioning system was a source of change of T_{amb} in the ~ 0.5°C range. This represented ~10% of the magnitude of the ascending phase of muscimol-induced increases in skin temperature at the hind paws and distal part of the tail and ~15% of the increases in skin temperature at the proximal tail. Therefore, the beginning (t_{min}) of the ascending phase of vasodilatation at the hind paws and distal part of the tail was calculated by considering the 10% percentile of ΔT_{skin}: $t_{min} = t_x - s \times \mathrm{Ln}(1/0.1\text{–}1)$ (Fig. 1*B*). A slightly different cutoff (15%) was chosen to estimate the onset of vasodilation at the proximal part of the tail, because of the slower evolution of the process at that location. The end (t_{max}) of the ascending phase of vasodilatation was calculated by considering the 90% percentiles of ΔT_{skin}: $t_x - s \times \mathrm{Ln}(1/0.9\text{–}1)$.

Then, the latency of the vasomotor reactions were divided into three groups according to the distribution of the beginning time t_{min} of the ascending phase of vasodilatation: $t_{min} < 7.5$ min, $7.5 < t_{min} < 15$ min and $t_{min} > 15$ min. This categorization was justified by the clear bimodal distribution of t_{min}, centered on 3–5 and 10–12 min, respectively (Fig. 1*C*). Beyond 15 min, the distribution of t_{min} was flat, and the observed effects if any were interpreted as resulting from uncontrolled diffusion of muscimol (Edeline et al. 2002). Together with a small volume of injection (50 nl) and a large number of negative sites of injection, this approach provided an acute delineation of the structures controling sympathetic cutaneous vasoconstrictor activity.

Three-dimensional mapping of response latencies. The large number of microinjection sites provided the opportunity of building a three-dimensional mapping of response latencies as a function of injection site, using interpolation. The interpolation was performed by computing an average of the responses obtained at all injection sites, weighted by the distance between the interpolated voxel and each injection site. This ensured that the interpolated values were most dependent on the responses of the nearest injection sites. In addition, because of the nonhomogeneous sampling of the interpolated volume, a mask was used to exclude voxels that were not close to at least one injection point.

For each measurement location (left paw, right paw, proximal tail, and distal tail), a three-dimensional (3D) volume representing response latencies as a function of injection site was obtained using interpolation. The responses obtained from the left and right paw were merged, by expressing the location of the injection site as ipsilateral (positive x-axis) vs. contralateral (negative x-axis) relative to the paw. The interpolated 3D volume extended from −2 to +2 mm along the x-axis, −1.5 to +1 mm along the y-axis, and −1 to +3.5 mm along the z-axis (200 points along each dimension). For each voxel of the volume, an interpolated latency was obtained by computing a weighted average of all latency values:

$$\text{latency}(x, y, z) = \frac{\sum w_i \text{latency}_i}{N}$$

The weight assigned for each latency value (w_i) was determined by the distance between the voxel (x, y, z) and the injection site (x_i, y_i, z_i):

$$w_i = \frac{1}{\left(\sqrt{(x_i - x)^2 + (y_i - y)^2 + (z_i - z)^2}\right)^6}$$

This weight is inversely proportional to the sixth power of the distance. This ensured that at any given location of the interpolated volume, interpolated latencies were more dependent on the latencies of the nearest injection site. Because the 3D volume was not homogeneously sampled (i.e., injection sites were clustered in some regions of the volume), a mask was used to exclude voxels, which were not located at a distance <0.5 mm of at least one injection point. Finally, because injection at a large amount of sites did not elicit any response, a second mask was computed to distinguish voxels located in regions where injection elicited a response from voxels located in regions where injection did not elicit a response after 55 min of recording. After assigning a latency of 55 min to these trials, the second mask was computed by taking all voxels of the interpolated volume having interpolated latencies above an arbitrary interpolated latency value of 53.5 min.

Heat loss index. The skin is an interface between T_{core} and T_{amb} acting as a radiator. In addition to active changes secondary to vasomotor tone of skin vessels, the temperature T of the skin can be affected passively by either T_{amb} or T_{core}. To cancel out these passive changes, we computed the heat loss index (HLI) = $(T_{skin} - T_{amb})/(T_{core} - T_{amb})$ as initially proposed by Székely (1986). The value of HLI can vary between 0 and 1, representing complete vasoconstriction ($T = T_{amb}$) and complete vasodilatation ($T = T_{core}$), respectively (Gordon et al. 2002; Romanovsky et al. 2002).

Analysis of vital signs. To study the systemic effects of muscimol on MAP, HR, $ETCO_2$, and T_{core} with respect to the microinjection sites, we divided the experiments in three groups on the basis of the beginning time t_{min} of the ascending phase of vasodilatation: *group 1*: $t_{min} < 15$ min for all considered skin areas either on the tail or the paws; *group 2*: $t_{min} < 15$ min for at least one but not all the areas considered on the tail or the hind paws; and group 3: $t_{min} > 15$ min for all considered skin areas either on the tail or the paws. The mean of each variable during the control period was considered as the reference level, and the temporal evolution was calculated in terms of variation of this level, namely T_{core} (Δ°C), MAP (ΔmmHg), HR (Δ°C), and $ETCO_2$ (Δ%).

Data processing and statistical analyses. The temporal evolution of the mean skin temperature, MAP, and HR was synchronized and measured with a 1-s time resolution. The corresponding time courses were downsampled to a 1-min time resolution by averaging. Data were expressed as means (±confident interval 95%). The comparisons were

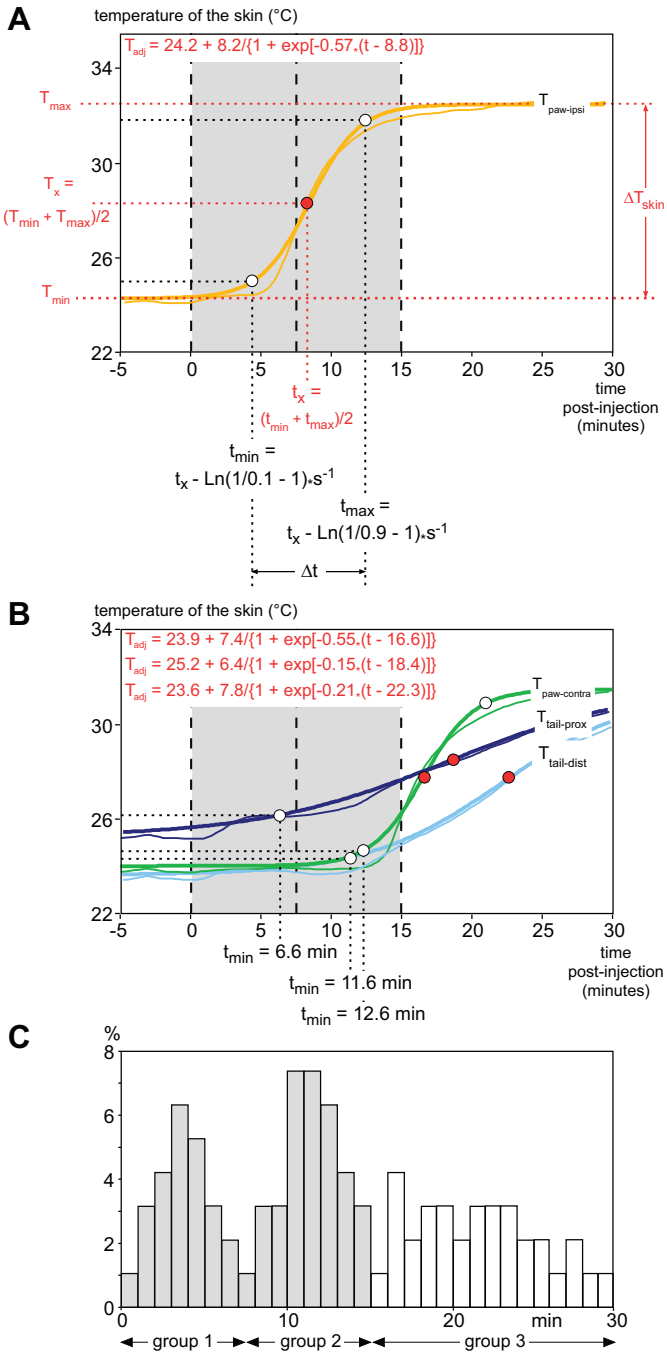

Fig. 1. Procedure to analyze the muscimol-induced variations of skin temperature. *A* and *B*, abscissa: time in minutes with reference to the end of the microinjection. Ordinate: temperature in °C. The grey area corresponds to the time intervals <7.5 and 7.5–15 min postinjection, delimited by vertical dotted lines. *A*: analysis of temperature variations observed from an ipsilateral hind paw ($T_{paw\text{-}ipsi}$). The thin yellow line is the temporal evolution of the temperature recorded during the 5-min control period and the following 30 min postinjection. The thick yellow line is the corresponding adjusted sigmoid Boltzmann curve $T_{adj} = T_{min} + \Delta T_{skin}/\{1 + \exp[-(t - t_x)]/s\}$, with $R^2 = 0.99$ (equation at *top left*). The adjusted parameters of the function are shown in red, namely the adjusted skin temperature during the control period ($T_{min} = 24.2$°C), the adjusted maximal skin temperature at the end of the process ($T_{max} = 32.4$°C), the amplitude of skin temperature variation ($\Delta T_{skin} = T_{max} - T_{min} = 8.2$°C), and the inflection point (t_x, $T_x = T_{min} + \Delta T_{skin}/2$) [(8.8 min, 28.3°C)] of the sigmoid represented by a red point. The beginning (t_{min}) and end (t_{max}) of the ascending phase of vasodilatation were then calculated by considering the 10 and 90% percentiles of ΔT_{skin}: $t_{min} = t_x - \text{Ln}(1/0.1-1) \times s^{-1} = 4.9$ min and $t_{max} = t_x - \text{Ln}(1/0.9-1) \times s^{-1} = 13.9$ min, represented by white points. *B*: calculation of the beginning of the ascending phase of vasodilatation observed from the corresponding three other recorded zones ($T_{paw\text{-}contra}$, $T_{tail\text{-}prox}$, and $T_{tail\text{-}dist}$). The thin and thick curves represent the genuine and adjusted curves, respectively. The green, dark blue, and light blue curves correspond to the contralateral hind paw, proximal and distal parts of the tail, respectively (corresponding equations provided at *top left*). Calculations of t_{min} were made as in *A*, except for the proximal part of the tail for which a 15% percentile was used in place of the 10% (see text). *C*: histogram showing the distribution of the beginning of the ascending phase of vasodilatation (t_{min}) for the ipsilateral hind paws, allowing the categorization into 3 groups: *group 1*: $t_{min} < 7.5$ min; *group 2*: $7.5 < t_{min} < 15$ min; *group 3*: $t_{min} > 15$ min.

done using the Mann-Whitney *U*-test and the Friedman repeated-measures ANOVA on ranks test.

RESULTS

The paws and tail of the rat were successfully maintained in vasoconstriction during the control period by preserving a stable, homogeneous, and constant surrounding temperature T_{warm}, adjusted to a few tenths degrees below T_{core}, and by keeping this temperature constant throughout the experiment. Following a 15-min period of control in steady vasoconstriction, muscimol (0.5 nmol, 50 nl) was injected over 60 s.

We will first describe in details a typical recording. Then the effects of muscimol will be detailed with reference to the injection sites determined postmortem. Emphasis will be made on the comparison between hind paws (ipsilateral vs. contralateral to the injection site). We seized the opportunity of the large number of microinjection sites to build 3D mappings of response latencies as a function of injection site, using interpolation. Results will also be synthesized by taking into account concomitant variations of MAP, HR, and T_{core}. Finally, the potential effect of muscimol on a widely used nociceptive test, the tail-flick test, will be assessed by using the present results to compute expected variations in tail-flick latency (TFL) elicited by the effects of muscimol on both tail temperature and T_{core}.

A typical example of the effects of muscimol microinjection within the RVM/rMR. An example of a thermographic film is provided as Supplemental Video S1 (Supplemental Material for this article is available online at the Journal website), from which a series of seven images recorded during 30 min are shown in Fig. 2*A*. These images correspond to a typical example of a microinjection centered to the RMg, as determined following histological examination (Fig. 2*H*). Figure 2*B* shows the temporal evolution of the temperature of *1*) the hind paws, ipsilateral ($T_{paw\text{-}ipsi}$) and contralateral ($T_{paw\text{-}contra}$) to the microinjection site; *2*) five sites on the tail; and *3*) a small piece of wood, indicator of T_{amb}. Figure 2*C* shows the temporal evolution of T_{core}. During the control period, T_{amb} and T_{core} were stable while the hind paws and tail were in vasoconstriction with skin temperatures slightly above T_{amb}. Following the injection of muscimol, a progressive increase of skin temperature is observed, starting at the ipsilateral paw ($T_{paw\text{-}ipsi}$: 4.9 min postinjection), followed by the proximal tail ($T_{tail\text{-}prox}$: 6.6 min), the distal tail ($T_{tail\text{-}dist}$: 11.6 min), and, finally, the contralateral paw ($T_{paw\text{-}contra}$: 12.6 min). The time courses of $T_{paw\text{-}ipsi}$ and $T_{paw\text{-}contra}$ were similar, increasing by 8.2 and 7.4°C, within 7.7 and 8.0 min respectively, and remaining stable afterwards. The temporal evolution of the temperature of the tail was quite different, taking 26.6 min to achieve a 6.4°C increase for $T_{tail\text{-}prox}$ vs. 21.2 min to achieve a 7.8°C increase for $T_{tail\text{-}dist}$. The intermediate parts of the tail showed a similar evolution whose parameters spread out between those of the extreme parts.

Shortly after vasodilatation of the ipsilateral hind paw, one sees a decrease in T_{core} (Fig. 2*C*) that was accentuated by the later vasodilation of the tail and contralateral hind paw. Overall, T_{core} was reduced by 0.8°C within the 30 min postinjection period despite the active warming that remained stable all over the experiment. The HLIs are shown in Fig. 2*D* for each site of T_{skin} skin recording.

MAP (Fig. 2*E*) and HR (Fig. 2*F*) were also affected by muscimol. Both parameters dropped and stabilized within 8 min, which is a few minutes earlier than the vasodilatation. At 30 min, the final MAP and HR were 36 and 20% less than during the control period, respectively. These variations were associated with a decrease of $ETCO_2$ (Fig. 2*G*).

From such an example, one can infer that microinjection of muscimol centered on the RMg is able to block the drive of the sympathetic control of vasomotion of the hind paws and the tail, leading to an increase in their skin temperature and a subsequent decrease in T_{core}. The effects were dominant on the part of the body ipsilateral to the microinjection site. These variations were associated with a decrease in MAP, HR, and $ETCO_2$.

Overall effect of muscimol microinjection within the RVM/rMR on the vasomotion of the hind paws. During the control period, both hind paws were vasoconstricted at a stable skin temperature, close to T_{amb}. The microinjection of muscimol in the RVM/rMR elicited an increase of the plantar skin temperature, indicating increasing blood flow. This reaction always started first in the ipsilateral hind paw. Following adjustment of each individual curve to a sigmoid by a Boltzmann regression (see Fig. 1, *A* and *B*), the experiments were divided in three groups on the basis of the distribution of the beginning (t_{min}) of the ascending phase of vasodilatation at the hind paw ipsilateral to the microinjection site (Fig. 1*C*): *group 1* (acute onset group: $t_{min} < 7.5$ min); *group 2* (intermediate onset group: $7.5 < t_{min} < 15$ min); and *group 3* (late onset or no response group: $t_{min} > 15$ min). The corresponding temporal evolutions of adjusted skin temperatures are shown in Fig. 3 for the three groups. Regarding the two groups showing responses with acute or intermediate onset, the ipsilateral and contralateral curves were essentially parallel, but the response elicited in the latter was postponed by 11–12 min. The ascending phase of vasodilatation Δt was short lasting (in the 6–8 min range) and large (in the 7–8°C/min range) and therefore steep (in the 1°C/min range). The corresponding numerical data are provided in Table 1.

Figure 4 shows the corresponding localization of the muscimol microinjection sites reported on the atlas of the rat brain by Paxinos and Watson (1986). For clarity of presentation, the data related to the hind paws, ipsilateral and contralateral to the microinjection sites, are shown on the Fig. 4, *A* and *B*, respectively. The black, grey, and white circles represent microinjection sites related to experiments belonging to the first, second, and third groups, respectively. Regarding the ipsilateral hind paw, the most effective sites are located between planes −1.3 and −2.8 mm with reference to the interaural line, mainly in raphe pallidus, inner layer of raphe magnus, and parapyramidal nucleus (Fig. 4*B*). These points are surrounded laterally and rostrocaudally by the second group (grey symbols), often localized in the outer layer of the raphe magnus. The nonreactive regions are outside these zones. The effects of microinjection on the contralateral hind paw (Fig. 4*A*) were very much dependent on its proximity to the midline. Microinjections distant from the midline by <0.1 mm exhibited an acute onset effect, and those by <0.3 mm an intermediate onset effect.

We seized the opportunity of the large number of microinjection sites to build a 3D mapping of response latencies as a function of injection site, using interpolation (Fig. 5). Since the effects were clearly lateralized, the responses obtained from

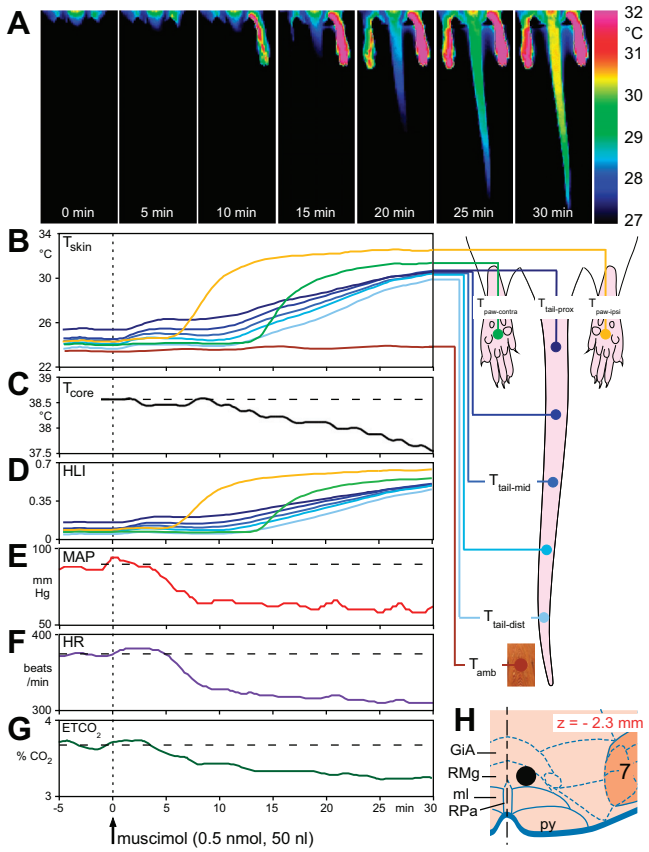

Fig. 2. Example of effects elicited by muscimol microinjection in the rostral ventromedial medulla (RVM). *A*: example of pictures taken at 0, 5, 10, 15, 20, 25, and 30 min postinjection of a thermographic movie recorded with a 320 × 240 pixel resolution (see the corresponding Supplemental Video S1). The false color scale of temperature is shown at *right*. *B*: temporal evolution of the temperatures recorded during the 5-min control and 30 min postinjection periods. Abscissa: time in minutes. Ordinate: temperature in °C. The 8 analyzed zones (10 pixels each) are indicated on the drawing at *right*. $T_{paw\text{-}ipsi}$ (yellow) and $T_{paw\text{-}contra}$ (green) corresponds to the skin temperature of the ipsi- and contralateral hind paw, respectively. $T_{tail\text{-}prox}$ (dark blue) and $T_{tail\text{-}dist}$ (light blue) corresponds to the skin temperatures of the proximal and distal part of the tail, respectively; there are 3 additional intermediate blue sites between these 2 sites. T_{amb} (brown) corresponds to the ambient temperature measured from a small piece of wood. Note the stability of the control period in vasoconstriction with skin temperatures near T_{amb}. Following the microinjection, the ipsilateral hind paw skin temperature raised first, followed by the proximal and distal parts of the tail and at last the contralateral hind paw. *C*: temporal evolution of core temperature (T_{core}). Abscissa: time in minutes. Ordinate: temperature in °C. Note the decrease in T_{core}, starting shortly after the rise of $T_{paw\text{-}ipsi}$. *D*: corresponding heat loss index [HLI = $(T_{skin} - T_{amb})/(T_{core} - T_{amb})$ (Romanovsky et al. 2002)] for the 7 skin areas considered. *E*: temporal evolution of mean arterial pressure (MAP). Abscissa: time in minutes. Ordinate: MAP in mmHg. Note the slight transitory increase in MAP shortly after the microinjection, followed by a sustained drop and then a progressive stabilization after 8 min postinjection. *F*: temporal evolution of heart rate (HR). Abscissa: time in minutes. Ordinate: HR in beat per minute (bpm). Note the slight transitory increase in HR shortly after the microinjection, followed by a sustained drop and then a progressive stabilization after 9 min postinjection. *G*: temporal evolution of $ETCO_2$. Abscissa: time in minutes. Ordinate: end tidal CO_2 ($ETCO_2$) in %. Note the parallel changes in *E*, *F*, and *G*. *H*: localization of the site of injection drawn on a frontal section of the brain in plane −2.3 mm caudal to the interaural line. The center of the injection site is located 0.3 mm lateral to the midline and 0.4 mm below the interaural line. 7, Facial nucleus; GiA, gigantocellular reticular nucleus pars alpha; ml, medial lemniscus; PPy, parapyramidal nucleus; py, pyramidal tract; RMg, raphe magnus nucleus; RPa, raphe pallidus nucleus.

the left and right paw were merged, by expressing the location of the injection site as ipsilateral (positive *x*-axis) vs. contralateral (negative *x*-axis) relative to the paw. The earliest responses latencies were observed between planes $z = -1.3$ and $z = -2.8$ mm both from the midline (raphe pallidus and raphe magnus) and a more lateral part centered on the lateral paragigantocellular nucleus (LPGi) and the parapyramidal nucleus (PPy).

Overall effect of muscimol microinjection within the RVM/rMR on the vasomotion of the tail. During the control period, the tail was vasoconstricted, with a decreasing thermal gradient from $T_{tail\text{-}prox}$ to $T_{tail\text{-}dist}$ [27.1 (26.9–27.3) vs. 24.9 (24.7–25.1)°C; $P < 0.001$]. The microinjection of muscimol within the RVM/rMR elicited an increase of the tail skin temperature. However, a proximal-distal gradient was also seen regarding the reactivity of the tail. Knowing these gradients, we analyzed the proximal and distal parts of the tail, separately, using the type of grouping already made but based on the starting point of the acute ascending phase of vasodilatation on the distal part of the tail [1st group (acute onset group): $0 < t_{min} < 7.5$ min; 2nd group (intermediate onset group): $7.5 < t_{min} < 15$ min; and 3rd group (late or none reactive): $t_{min} > 15$ min], following sigmoidal adjustment of each individual. The corresponding

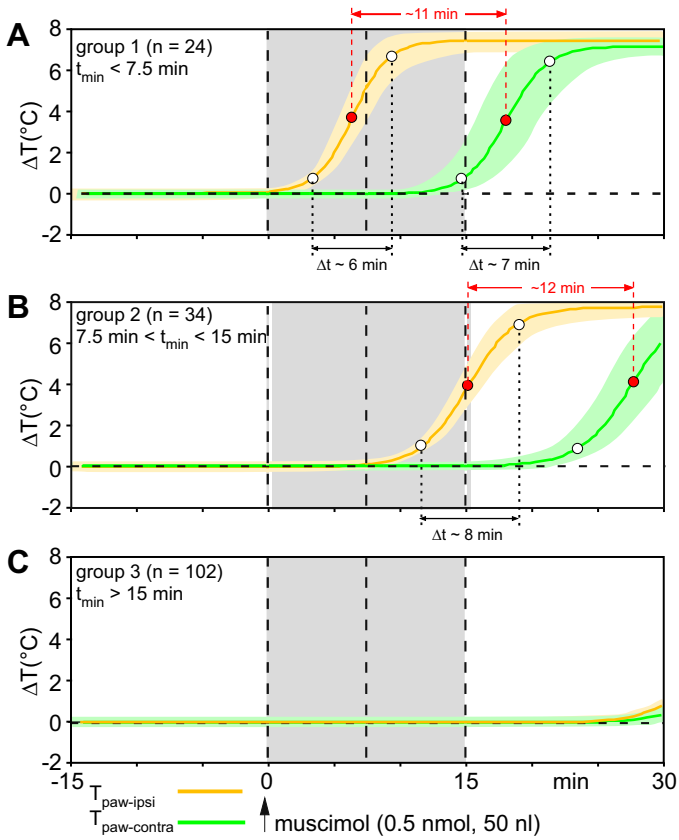

Fig. 3. Temporal evolution of the skin temperature recorded from the hind paws, following muscimol microinjections. Abscissa: time in minutes. Ordinate: temperature variation in °C (mean ± 95% confidence interval). As indicated at *bottom left*, yellow and green curves are data adjusted to a Boltzmann sigmoid (see Fig. 1) from the ipsi ($T_{paw\text{-}ipsi}$)- and contralateral ($T_{paw\text{-}contra}$) hind paw skin temperature, respectively. The experiments were divided in 3 groups on the basis of the distribution of the beginning (t_{min}) of the ascending phase of vasodilatation from the ipsilateral hind paw. *A*: *group 1*: $t_{min} < 7.5$ min. *B*: *group 2*: $7.5 < t_{min} < 15$ min. *C*: *group 3*: $t_{min} > 15$ min. See text and Table 1.

temporal evolutions of adjusted skin temperatures are shown in Fig. 6 for the three groups. Regarding the first two groups, the corresponding numerical data are provided in Table 1. By comparison with the paws the process was slower (in the 0.3–0.5°C/min range) and less pronounced (in the 4–6°C range), possibly because we recorded the dorsal facet of the tail (see DISCUSSION).

Figure 7 shows the corresponding localization of the muscimol microinjection sites for the proximal (Fig. 7*A*) and the distal (Fig. 7*B*) parts of the tail. Again, the black grey and white symbols represent the acute, intermediate, and late or none reactive group respectively. The black symbols are located mainly between planes −1.3 and −2.8 mm, close to the midline, in the raphe pallidus and raphe magnus. The grey symbols surround the black ones and are located in the raphe magnus and parapyramidal region. In these two groups, the proximal and distal parts of the tail reacted concomitantly. Overall, the proximal part of the tail was more responsive to the microinjection; in particular, one can see several points from which a vasodilatation was elicited on the proximal but not on the distal part of the tail, at least within the 15-min early period. Most of these points were however, located in the raphe magnus and parapyramidal nucleus.

Figure 8 represents the 3D mapping of response latencies t_{min} as a function of injection site. For both the proximal (Fig. 8*A*) and the distal (Fig. 8*B*) parts of the tail, the earliest response latencies were observed between planes $z = -1.3$ and $z = -2.8$ mm from the midline (raphe pallidus and raphe magnus) and a more lateral part. Interestingly, the lateral part centered on the parapyramidal nucleus was restricted to planes $z = -2.3$ to -2.8 mm without any obvious participation of the lateral paragigantocellular nucleus.

Comparison of heat loss indexes in various vasomotor states. The potential extent of skin temperature variations was physically restricted to the T_{amb}-T_{core} range. In terms of thermoregulation, these changes are best described using the Heat Loss Index as it eliminates the passive changes and range limitation due to any T_{amb} and T_{core} variations (Gordon et al. 2002; Romanovsky et al. 2002; Székely 1986): $HLI = (T_{skin} - T_{amb})/(T_{core} - T_{amb})$. Table 2 compares results of skin temperature, converted in terms of HLI, obtained in the present study (acute onset *group 1*, black symbols) to previous experiments performed on anesthetized rats maintained in thermoneutral conditions (El Bitar et al. 2014a). The HLI values in the control period of the present study were close to those recorded during vasoconstrictions in our previous study and identical in terms of ranking ($T_{tail\text{-}dist} < T_{paw\text{-}ipsi} < T_{tail\text{-}prox}$). However, the HLI values following muscimol microinjection were 20–25% lower than the HLI seen during the maximal physiological vasodilatation achieved during thermoneutrality. This observation suggests that the ongoing hind paws and tail fiber sympathetic activity was not completely silenced following the muscimol microinjections, in spite of an apparent ceiling effect.

Overall results, including the effects on vital signs. To homogenize the results for further analyzes, the experiments were reorganized in three new groups, again on the basis of the onset time t_{min} of the ascending phase of vasodilatation (Fig. 9). The first includes experiments where t_{min} was < 15 min for all considered skin areas either on the tail or the paws (black circles in Fig. 9*A*). They were located between planes −0.8 and −2.8 mm, not more lateral than 0.3 mm from the midline, mainly in the inner part of raphe magnus and raphe pallidus. The second includes experiments where t_{min} was < 15 min for at least one but not all the areas considered on the tail or the hind paws (grey circles in Fig. 9*A*). They were located in the raphe magnus and parapyramidal area, surrounding the preceding group. The third group includes experiments where t_{min} was > 15 min for all considered skin areas either on the tail or the paws (white circles in Fig. 9*A*). The corresponding effects of microinjection of muscimol on $T_{paw\text{-}ipsi}$, $T_{paw\text{-}contra}$, $T_{tail\text{-}prox}$, and $T_{tail\text{-}dist}$ are summarized in Fig. 9, *B*, *C*, *D*, and *E*, respectively.

Figure 9*F* shows the concomitant effects on T_{core}. There was no statistical difference among the three groups concerning T_{core} during the control period ($P = 0.94$). After the muscimol

Table 1. *Results of paws (see Fig. 3) and tail (see Fig. 6)*

	T_{min}, °C	ΔT_{skin}, °C	t_{min}, min	t_x, min	Δt, min	$\Delta T_{skin}/\Delta t$, °C/min
Paw						
Ipsilateral						
Group 1	25.4 (25.2–25.7)	7.4 (7.2–7.7)	3.6 (3.4–3.8)	6.6 (7.4–5.8)	6.6 (7.4–5.8)	1.2 (1.0–1.6)
Group 2	25.4 (25.2–25.7)	7.7 (7.4–8.0)	11.3 (11.2–11.5)	15.3 (16.0–14.6)	7.9 (6.7–9.0)	7.9 (6.7–9.0)
Contralateral						
Group 1	25.6 (25.5–25.8)	7.2 (7.0–7.4)	14.6 (12.8–16.3)*	18.0 (15.8–20.2)*	6.8 (5.9–7.7)	1.1 (0.9–1.3)
Group 2	25.4 (25.3–25.6)	7.9 (7.6–8.2)	23.5 (22.0–25.0)*	27.8 (29.6–25.9)*	8.5 (7.8–9.2)	0.9 (0.8–1.0)
Tail						
Proximal						
Group 1	27.7 (27.4–28.0)	4.4 (4.1–4.7)†	2.4 (2.4–2.5)†	8.1 (8.9–7.2)	14.2 (11.9–16.5)†	0.3 (0.2–0.4)†
Group 2	27.7 (27.3–28.2)	4.4 (4.0–4.9)†	8.2 (8.1–8.4)†	16.1 (16.9–15.3)	15.7 (13.7–17.7)†	0.3 (0.2–0.4)†
Distal						
Group 1	25.2 (25.0–25.5)	5.6 (5.2–6.0)†	2.4 (2.0–2.8)†	8.6 (7.1–10.2)†	14.7 (11.2–18.2)†	0.4 (0.3–0.5)†
Group 2	25.4 (25.0–25.8)	6.2 (5.7–6.7)†	11.2 (11.0–11.4)	17.5 (18.6–16.4)†	12.5 (10.7–14.4)†	0.5 (0.4–0.6)†

Results (expressed as means ± confident interval 95%) obtained following Boltzmann sigmoid regression of individual curves of skin temperature following microinjections of muscimol (see Fig. 1). For both the paws and the tail, the experiments were divided in 3 groups on the basis of the beginning time t_{min} of the ascending phase of vasodilatation. *Group 1*: t_{min} <15 min for all skin areas; *group 2*: t_{min} <15 min for at least 1 skin area; *group 3* (not shown): t_{min} >15 min for all skin areas (see Fig. 3 and 6). t_x, Abscissa of the inflection point of the sigmoid; Δt, duration of the ascending phase of vasodilatation; T_{min}, adjusted skin temperature during the control period; ΔT_{skin}, amplitude of skin temperature variation; $\Delta T_{skin}/\Delta t$, speed of warming. The regression coefficients R^2 of the adjusted curves were always highly significant (> 0.98). *$P < 0.01$, with respect to the corresponding value of the ipsilateral paw. †$P < 0.05$, with respect to the corresponding value of the ipsilateral paw.

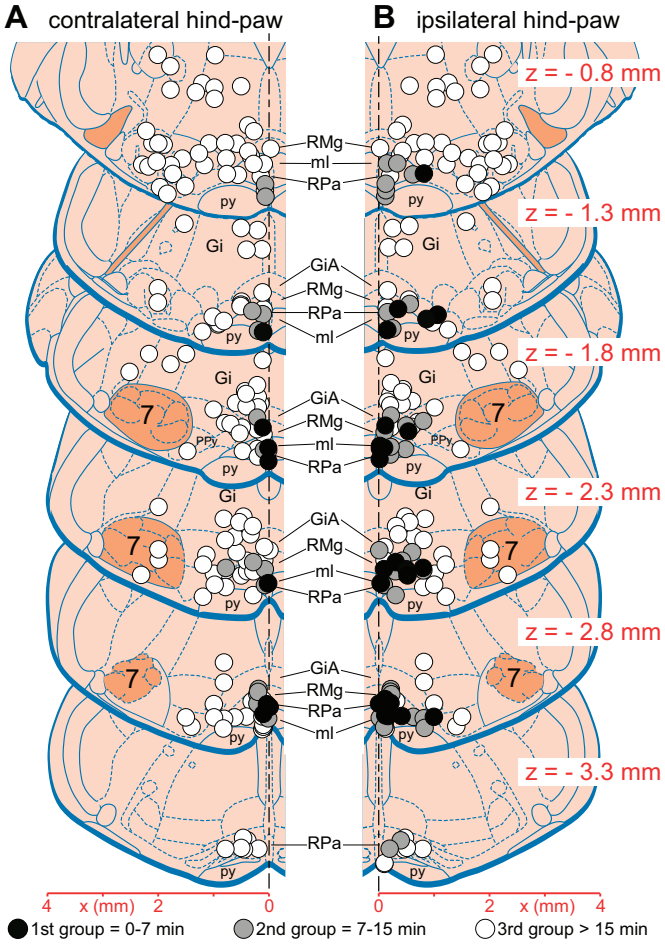

Fig. 4. Overall effects elicited by muscimol microinjection on the skin temperature recorded from the hind paws. *A*: contralateral hind paw. *B*: ipsilateral hind paw. Schema of frontal sections of the brain from interaural $z = -0.8$ (*top*) to $z = -3.3$ mm (*bottom*), based on the stereotaxic atlas by Paxinos and Watson (1986). The circles indicate the center of the corresponding injection sites, with a diameter scaled to a 50-nl sphere. The black symbols represent the early latency group with an onset of vasodilatation in <7.5 min. The grey symbols correspond to the intermediate latency group with an onset of vasodilatation between 7.5 and 15 min. The white symbols stand for the group that included the experiments with an onset of vasodilatation in >15 min (or did not react at all).

injection, the mean temperatures diverged strongly with progressive drops for the first and second group. The effects of muscimol microinjections on MAP, HR, and $ETCO_2$ are presented in Fig. 9, *G*, *H*, and *I*, respectively. For all three groups, we report a transitory increase of MAP and HR in the first minute following the microinjection of muscimol. Thereafter, the curves declined slowly and slightly till the end of the experiments. Regarding the first two groups, the corresponding numerical data are provided in Supplemental Table S1. These results are in line with previous reports in anesthetized rats following microinjection of muscimol in the RVM/rMR, describing slight or nonsignificant decreases in MAP, HR, and $ETCO_2$ (Bernard et al. 2008; Blessing and Nalivaiko 2001; Nakamura and Morrison 2007; Tanaka et al. 2007; Zaretsky et al. 2003a,b). Note that our recordings were made under an anesthetic regime that preserves withdrawal reflexes while most earlier reports were obtained with deeper regimes that could have masked the effects reported here.

Modeling the effect of muscimol injection within the RVM/rMR on the tail-flick test. In a previous study, we proposed and verified experimentally a simple model to compute the expected TFL of a rat exposed to a source of radiant heat applied onto the tail (Benoist et al. 2008). The model takes into account the power of the radiant heat source, the initial skin temperature, T_{core}, and the site of stimulation on the tail and has been applied successfully to reconstruct TFLs following a conditioned stress response (Carrive et al. 2011). Here, the model was used to compute the predictable variations of TFL introduced by muscimol. Decisional and motor latencies were estimated to be 134 and 4 ms, respectively (Benoist et al. 2008). Considering a site of stimulation on the mid-tail, the distance to the dorsal horn entry zone is ~200 mm. The model provides the following equation for the expected tail-flick latency: $TFL\ (s) = [(36.8 - 0.73 \times T_{mid\text{-}tail})^2/\alpha + 90/(0.041 \times T_{core} - 0.47) + 110/(0.041 \times T_{mid\text{-}tail} - 0.47) + 138]/1{,}000$ where α is the slope of the squared temperature variation (in $°C^2/s$) generated by the power of the radiant heat source.

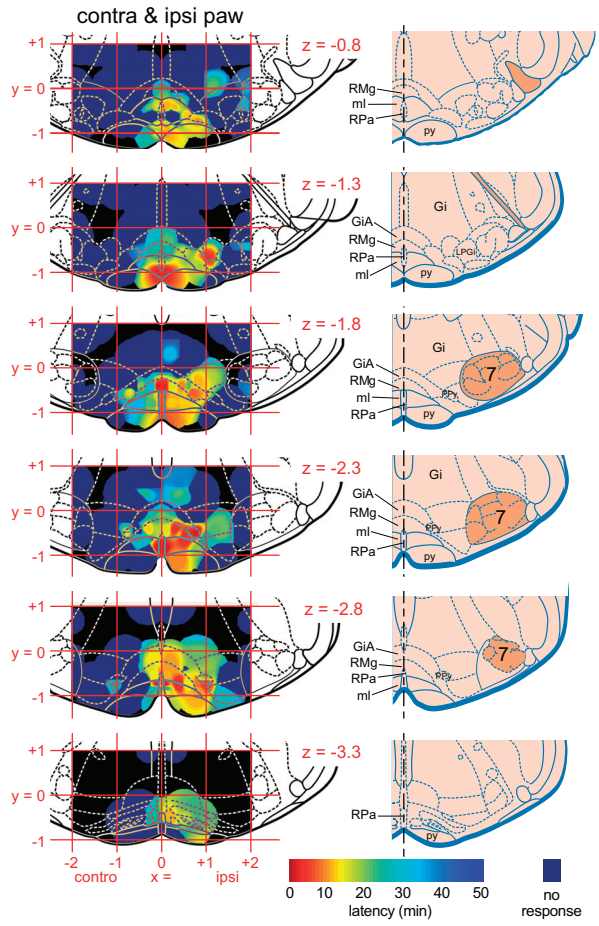

Fig. 5. Three-dimensional mapping of the hind paw response latencies t_{min} as a function of injection sites. The responses obtained from the left and right paw were merged by expressing the location of the injection site as ipsilateral (positive *x*-axis) vs. contralateral (negative *x*-axis) relative to the paw. *Left*: interpolated response latencies are indicated by the false colors (scale shown at *bottom right*). They are adjusted on frontal sections of the brain from interaural $z = -0.8$ (*top*) to $z = -3.3$ mm (*bottom*) with *y* being the ventrodorsal coordinate, again with reference to the interaural line. *Right*: drawings are based on the stereotaxic atlas by Paxinos and Watson (1986).

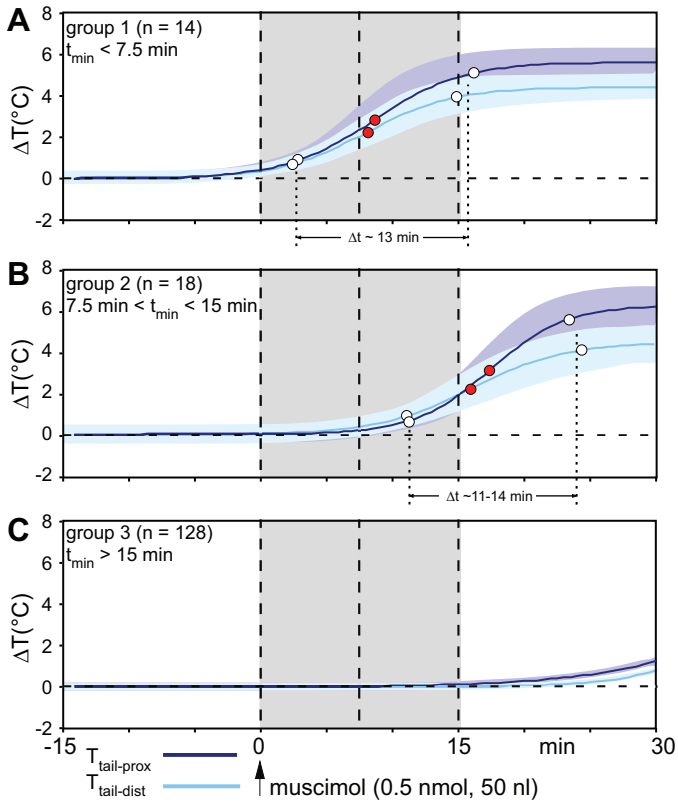

Fig. 6. Temporal evolution of the skin temperature recorded from the tail, following muscimol microinjections. Abscissa: time in minutes. Ordinate: temperature variation in °C (mean ± 95% confidence interval). As indicated at *bottom left*, dark blue and blue colors are data adjusted to a Boltzmann sigmoid (see Fig. 1) from the skin temperature of the proximal ($T_{tail\text{-}prox}$) and distal ($T_{tail\text{-}dist}$) part of the tail, respectively. The experiments were divided in 3 groups on the basis of the distribution of the beginning (t_{min}) of the ascending phase of vasodilatation on the distal part of the tail. *A*: *group 1*: $t_{min} < 7.5$ min. *B*: *group 2*: $7.5 < t_{min} < 15$ min. *C*: *group 3*: $t_{min} > 15$ min. See text and Table 1.

Let us recall at this point that, when the skin is exposed to a constant power source of infrared radiation, the temperature increases with the square root of time, according to the law of radiant heat transfer $T = T_{mid\text{-}tail} + a.t^{0.5}$ or expressed in terms of temperature variation $T - T_{mid\text{-}tail} = a.t^{0.5}$. This quadratic relationship becomes linear in t by squaring the two terms of the equation: $(T - T_{mid\text{-}tail})^2 = a^2.t = \alpha.t$ where α is the slope of the squared temperature variation generated by the power of the radiant heat source [see Fig. 2*A* in Benoist et al. (2008)]. The predictive model of TFL was fully verified following variations of the radiant heat source (i.e., α) or the basal temperature of the skin (i.e., $T_{mid\text{-}tail}$ here) [see Fig. 8 in Benoist et al. (2008)]. In the classical tail-flick test, the principal source of variation introduced by experimenters is the power of the electrical bulb used for heating the skin of the animal. The investigator adjusts the radiant heat emission with a rheostat to achieve a predetermined TFL in the control situation, most commonly in the 2- to 4-s range (Le Bars et al. 1999, 2009). In the model, such latencies are achieved for α in the $0.08-0.2°C^2/s$.

The model was applied to the data of animals in which the beginning of the ascending phase of vasodilatation was <15 min either on the tail or the paws (black group in Fig. 9). The model foretells a 30–35% decrease of the TFL, 30 min following muscimol administration (Fig. 10). It appears therefore that, regardless of any other additional possible causes, the vasodilatation of the tail is a major source of variation of the TFL following muscimol administration in RVM/rMR.

DISCUSSION

Muscimol was injected in the lower brainstem with the aim of assessing the role of the RVM/rMR on the control of sympathetic drive to the tail and hind paws. Microinjections within this brainstem region increased the skin temperature of the hind paws and tail as a result of reduced vasomotor tone. The effects were dominant on the hind paw ipsilateral to the microinjection site. Increased heat loss through vasodilatation of the tail and paws was associated with a drop of T_{core} and slight decreases of MAP, HR, and $ETCO_2$.

Following some technical considerations regarding the microinjection procedure, we will discuss the following points: *1*) general findings; *2*) lateral localization of effective sites; *3*) rostrocaudal localization of effective sites; and *4*) pharmacological manipulations of RVM/rMR in pain studies.

Technical considerations regarding the microinjection procedure. The kinetic and volume of efficient microinjection are determined by numerous factors: the concentration, rate of delivery, and properties of both the drug (coefficient of diffusion, binding, catabolism) and the tissue (volume fraction,

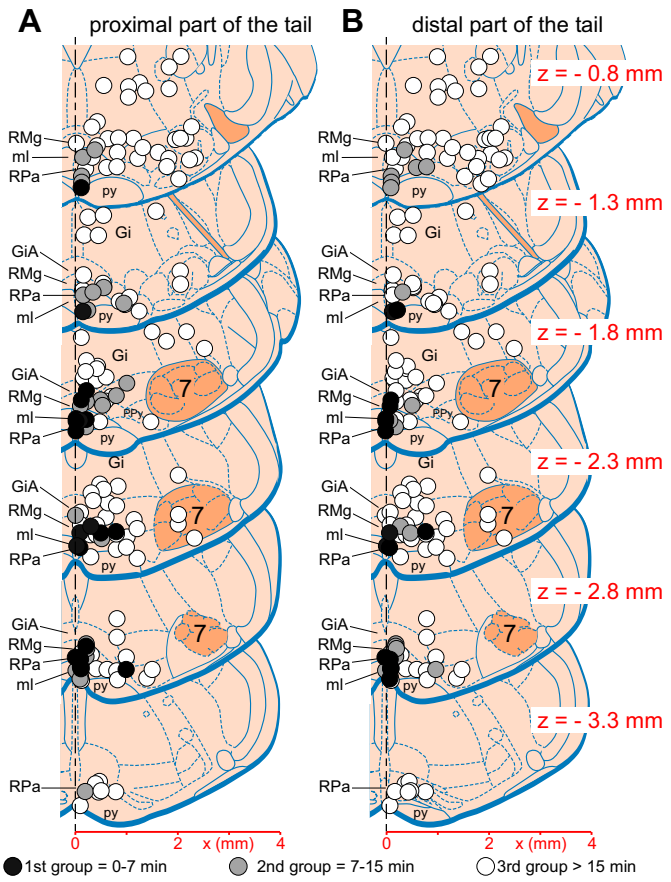

Fig. 7. Overall effects elicited by muscimol microinjection on the skin temperature recorded from the tail. *A*: proximal part of the tail. *B*: distal part of the tail. Symbols and abbreviations as in Fig. 4.

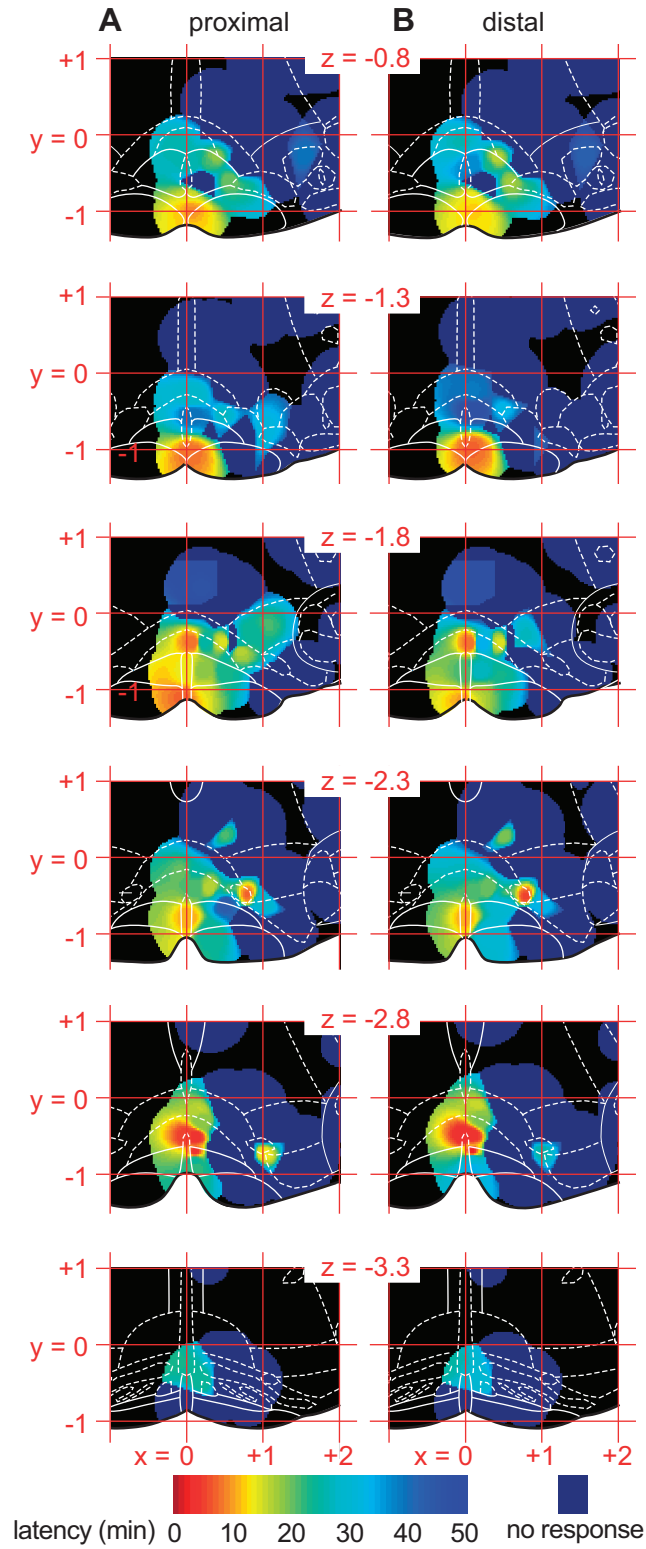

Fig. 8. Three-dimensional mapping of the tail response latencies t_{min} as a function of injection sites. *A*: proximal part of the tail. *B*: distal part of the tail. The interpolated response latencies are indicated by the false colors (scale shown at *bottom*). They are adjusted on frontal sections of the brain from interaural $z = -0.8$ (*top*) to $z = -3.3$ mm (*bottom*) with x and y being the lateral and ventrodorsal coordinate, respectively, again with reference to the interaural line. Symbols and abbreviations as in Fig. 5.

tortuosity) (Syková and Nicholson 2008). In nuclear and cortical homogenous regions, drug distributions are typically spherical or in the shape of drop (Bondareff et al. 1970; Martin 1991; Myers 1966).

In a "mapping" study aiming at demarcating a functional region in the brain, both positive and negative results are significant. A negative result obtained with a large dose is a very convincing result in this respect. Considering the large volume of the explored brain structure (roughly $3 \times 4 \times 2 = 24$ mm^3), a compromise was necessary to both find significant positive results with minimal doses and to avoid useless negative results. Studies on the involvement of these regions in pain/nociception and thermoregulation have used muscimol injections in the 10- to 1,000-pmol/60- to 1,000-nl ranges (Bernard et al. 2008; Blessing and Nalivaiko 2001; Brink et al. 2006; Cao et al. 2004, 2010; Cerri et al. 2010; Fan et al. 2007. Gilbert and Franklin 2001; Heinricher and Kaplan, 1991; Martenson et al. 2009. Meng et al. 1998; Morrison 1999, 2003; Nakamura and Morrison 2007, 2011; Ootsuka and McAllen 2005; Rathner et al. 2008; Vianna et al. 2008; Zaretsky et al. 2003a,b). Knowing that muscimol does not spread appreciably because it is a potent ligand for neuronal and glial $GABA_A$ receptors, we decided to use a small volume of injection (50 nl = 0.05 mm^3, that is a ~0.5 mm diameter for an ideal sphere) but a relatively high concentration. This was supposed to provide an effective radius of blockade in the ~1-mm range (Martin 1991; Martin and Ghez 1999; Malpeli 1999; Edeline et al. 2002). Following similar microinjections using [^{3}H]muscimol, autoradiographic analyses showed a spread ~1.5 mm from the injection site at 15 min (Edeline et al. 2002; Martin 1991). Martin and Ghez (1999) used glucose metabolism to assess the extent of inactivation and observed a central core of blockade (~1-mm radius) surrounded by an extensive region of reduced metabolism, possibly due to reduced synaptic activity of neurons receiving projections from the core region. In summary, muscimol binds strongly and diffuses slowly outward at effective concentrations from the region immediately inundated by the bulk flow (Malpeli 1999).

Since myelinated fiber bundles impede muscimol diffusion (Allen et al. 2008), it is likely that the particular architecture of the RVM/rMR with a predominance of rostrocaudal fibers and a low neuronal density favors a rostrocaudal diffusion of the product. In addition, the two paired bundles of myelinated fibers that cover the brainstem floor, namely the pyramidal tract and the medial lemniscus, constitute a strong diffusion barrier. Accordingly, the postmortem examination of pontamine spread revealed an elongated pattern of diffusion two times longer in the rostrocaudal direction compared with the coronal plane.

Using these microinjections, we were able to build response maps on the basis of 160 experiments. Together with the small volume of injection and the large number of negative sites of injection (60%), this approach provided *1*) an acute delineation of the structures able to block sympathetic cutaneous vasoconstrictor activity; *2*) the possibility of a temporal analysis of these effects; and *3*) the resultant capacity of defining a brain region as the core of effects, surrounded by intermediate and then ineffective zones.

Because of such a large number of injection sites, we introduced a new procedure to compute 3D interpolated maps of response latencies and overall sympathetic blockade as a

Table 2. *Summary of skin vasomotor tone*

	HLI During Vasoconstriction			HLI During Vasodilation		
	Control period (present study)	Vasoconstriction periods (El Bitar et al. 2014a)	*P*	30 min following muscimol	Vasodilation periods (El Bitar et al. 2014a)	*P*
$T_{paw\text{-}ipsi}$	0.10 (0.10–0.11)	0.13 (0.09–0.16)	0.12	0.69 (0.65–0.74)	0.92 (0.85–0.98)	< 0.00001
$T_{tail\text{-}prox}$	0.24 (0.22–0.25)	0.23 (0.21–0.26)	0.64	0.62 (0.57–0.67)	0.77 (0.72–0.83)	< 0.0001
$T_{tail\text{-}dist}$	0.04 (0.04–0.04)	0.03 (0.01–0.05)	0.06	0.55 (0.46–0.63)	0.74 (0.69–0.80)	< 0.0001

Results are expressed in terms of heat loss index [HLI = $(T_{skin} - T_{amb})/(T_{core} - T_{amb})$] (Gordon et al. 2002; Romanovsky et al. 2002; Székely 1986), represented as means and their 95% confidence interval. Results obtained from current study are compared to a previous study in the extreme vasomotor tone status, namely vasoconstriction and vasodilation. During vasoconstriction, there were no significant statistical differences between HLI observed in the 2 studies. By contrast, the HLI for both hind paws and following muscimol microinjections were significantly lower than the HLI seen during the physiological vasodilation elicited during thermoneutrality (El Bitar et al. 2014a).

function of injection site. The interpolation was performed by computing an average of the responses obtained at all injection sites, weighted by the distance between the interpolated voxel and each injection site. This ensured that the interpolated values were most dependent on the responses of the nearest injection sites. In addition, because of the nonhomogeneous sampling of the interpolated volume, a mask was used to exclude voxels that were not close to at least one injection

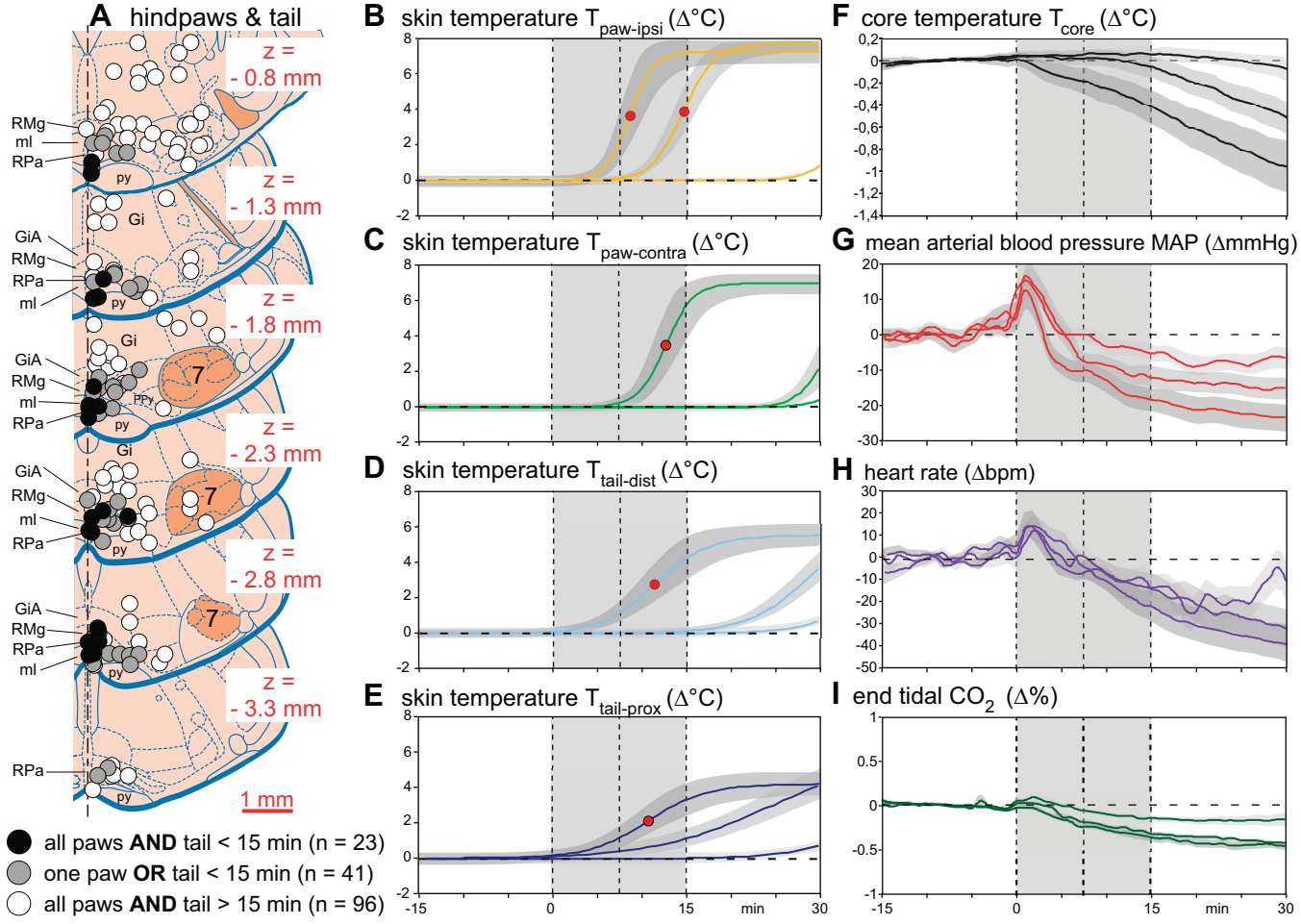

Fig. 9. *A*: schema of frontal sections of the brain from interaural −0.8 (*top*) to −3.3 mm (*bottom*). Symbols and abbreviations as in Fig. 4. The data were synthesized by regrouping the experiments in 3 new groups, again on the basis of the beginning time t_{min} of the ascending phase of vasodilatation, considering all skin areas either on the tail or the paws. The black symbols represent the early latency group with $t_{min} < 15$ min for all considered skin areas either on the tail or the paws. The grey symbols correspond to the intermediate latency group with $t_{min} < 15$ min for at least 1 of these areas. The white symbols correspond to the late latency group with $t_{min} > 15$ min for all considered skin areas. *B*: variation of skin temperature (Δ°C) recorded from the ipsilateral hind paw. *C*: variation of skin temperature (Δ°C) recorded from the contralateral hind paw. *D*: variation of skin temperature (Δ°C) recorded from the distal part of the tail. *E*: variation of skin temperature (Δ°C) recorded from the proximal part of the tail. *F*: variation of T_{core} (Δ°C). In the 1st group, T_{core} declined linearly as early as the first minute postinjection; for the 2nd group, T_{core} decline is parallel to the 1st group's but with 15-min delay and the 3rd group's T_{core} remained stable. *G*: variation of mean arterial blood pressure (ΔmmHg). Note a slight transitory increase of MAP in all groups, shortly after the microinjection followed by a sustained drop. This was followed by a slow decline in the first group, stabilization in the 3rd group, while the 2nd group spread out in between. *H*: corresponding variations of heart rate (Δbpm). *I*: variation of $ETCO_2$ (Δ%). The corresponding numerical data are provided in Supplemental Table S1.

point. The obtained volumes provide an interesting mean to assess the relationship between the effects of the injection and the anatomical location of the injection.

General findings. Our results are largely in agreement with earlier reports regarding the sympathetic drive of the tail. Microinjection of glycine, GABA, or muscimol in the RVM/rMR blocks the activation by cold or fever of sympathetic fibers that innervate the tail (Blessing and Nalivaiko 2001; Cerri et al. 2010; Korsak and Gilbey 2004; Ootsuka and McAllen 2005; Ootsuka et al. 2004; Rathner et al. 2008; Vianna et al. 2008). On the other hand, microinjection of glutamate or bicuculline increases the activity of vasomotor sympathetic nerves of the tail, thus decreasing the blood flow, without affecting the mesenteric vascular bed (Blessing and Nalivaiko 2001; Morrison 2001; Rathner and McAllen 1999). Several aspects of our contribution should be highlighted.

The experimental conditions were close to those of thermoneutrality (El Bitar et al. 2014a). T_{warm} was adjusted to ~0.3°C below T_{core}. Demonstrating their vasoconstricted state, the temperature of the distal part of the tail was very close to the ambient temperature (~0.7°C above T_{amb}). It then increased by ~6°C following the injection of muscimol in responsive brainstem sites. In comparable experimental conditions, microinjection of GABA or muscimol in RVM/rMR blocks the activity of the sympathetic fibers innervating the rat tail (Korsak and Gilbey 2004; Ootsuka and McAllen 2005).

We have previously discussed (El Bitar et al. 2014a) that the vasomotor tone of the dorsal facet of the tail is less reactive than the ventral facet, notably because the ventral artery is larger than the lateral arteries, while the ventral vein is thinner than the lateral veins (Knoppers 1942; Thorington 1966; Wu et al. 1995; Young and Dawson 1982). It follows that the temperatures of the dorsal and ventral facets of the tail are identical during vasoconstriction but shift by ~3°C during full vasodilatation. The recorded effects from the tail were thus underestimated, compared with those seen on the hind paws.

A major novelty of our study was to include the paws to these basic phenomenological observations. Such as for the tail, the hind paws were in a stable vasoconstricted state, as demonstrated by the fact that the temperature of the hind paws was close to the ambient temperature (2–3°C above T_{amb}). This increased by ~7°C following the injection of muscimol in the active sites. We have already discussed the involvement of the paws in rat thermoregulation (El Bitar et al. 2014a). The feet make up ~10% of the total surface area of the body, slightly more than the tail (Lin et al. 1979). It follows that the substantial muscimol-induced vasodilatation of the paws contributed significantly to T_{core} drop (~1°C within half an hour).

Our purpose was not to confirm well-documented notions. We specifically aimed at mapping the brainstem regions that contain the premotor sympathetic neurons that control the vasomotor tone of the tail and hind paws because most models of pain/nociception are based on behavioral responses elicited by thermal stimulation (reviewed in Le Bars et al. 2001, 2009). We undertook this large study because studies on pain/nociception have emphasized the RVM, which includes the nucleus raphe magnus and the gigantocellular reticular nucleus pars alpha (mainly at the level of the facial nucleus), while studies on thermoregulation have emphasized a slightly shifted more caudal region centered on the raphe pallidus. In addition, we described in a previous work that neurons involved in pain/nociception located in the brainstem are probably also implicated in autonomic regulation, notably cutaneous vasomotion (El Bitar et al. 2014b).

The results of the present study suggest that the regions described as being involved in pain/nociception modulation and the regions involved in thermoregulation are spatially matched, at least functionally regarding the vasomotor tone of the tail and hind paws.

Localization of effective sites in coronal planes. The most effective sites were restricted to well-circumscribed regions. Numerous negative microinjections sharpened the delineation. Our observations regarding the tail are in keeping with the mapping by Korsak and Gilbey (2004), who reported that GABA microinjections in the region of raphe pallidus and magnus markedly decreased the sympathetic cutaneous vasoconstrictor activity in the dorsal collector nerves of the tail, while injections more dorsal or lateral tended to produce either a smaller decrease or have no effect. Blessing and Nalivaiko (2001) also emphasized the raphe magnus, raphe pallidus, and parapyramidal nucleus in this respect, although they did not provide a graphical mapping of the effects.

Only microinjections in RMg, RPa, and PPy elicited a vasodilatation in the ipsilateral hind paw within <7.5 min, and those distant from the midline by <0.3 mm induced a vasodilatation in the contralateral hind paw within the same period. These observations deserve two comments. First, within the coronal plane, the lateral diffusion of muscimol was limited, as expected. Second, projections of RVM/rMR cells are mainly

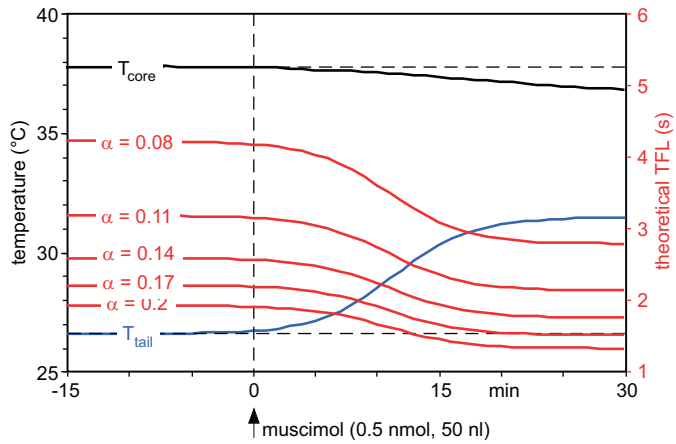

Fig. 10. We proposed and verified experimentally a simple model for computing the tail-flick latency (TFL) in the rat, taking into account the power of the radiant heat source, the initial temperature of the skin, T_{core}, or the site of stimulation on the tail (Benoist et al. 2008). This model is used here to compute the predictable variations of the TFL introduced by muscimol in the positive cases of the present experiments. Since the decisional and motor latencies were estimated 134 and 4 ms, respectively (Benoist et al. 2008) and considering a site of stimulation on the mid-tail far-off the dorsal horn entry zone by 200 mm, the model provides the following equation giving the tail-flick latency: $TFL\ (s) = [(36.8 - 0.73 \times T_{mid\text{-}tail})^2/\alpha + 90/(0.041 \times T_{core} - 0.47) + 110/(0.041 \times T_{mid\text{-}tail} - 0.47) + 138]/1{,}000$, where α is the slope of the squared temperature variation, witness of the power of the radiant heat source. Experimental data are from the experiments where the beginning of the ascending phase of vasodilatation was <15 min either on the tail or the paws (black group in Fig. 9); they include both the mean temperatures of the core (T_{core}, brown line) and the middle of the tail ($T_{mid\text{-}tail}$, blue line). In the control situation, the model provides TFLs (red lines) in the 2–4 s range for α in the 0.08–0.2°C^2/s range: the model foretells a 30–35% decrease of the TFL following muscimol microinjections in the sites indicated by a black circle in Fig. 9*A*.

lateralized, predominantly controlling vasomotor tone of the ipsilateral body side. Our results are in keeping with studies showing that RVM/rMR neurons send axons towards the spinal cord mainly through the ipsilateral dorsolateral funiculus (Basbaum and Fields 1979; Fields et al. 1995; Lefler et al. 2008; Light 1985). Microinjections close to the midline also elicited early vasodilatation of the tail, the most effective sites being restricted to the same well-circumscribed regions. Neurons in the PPy present morphological, histochemical (Helke et al. 1989; Lynn et al. 1991) and functional (Blessing and Nalivaiko 2000) properties similar to those of the RPa. Some authors therefore consider PPy as part of RPa (e.g., Cano et al. 2003).

Interestingly, brainstem neurons activated both antidromically from the lumbar dorsolateral funiculus and by mild cooling of the animal T_{core} were found in both raphe pallidus and magnus (Rathner et al. 2001). Such neurons could be involved in the results presented here. However, there are other control loops that regulate the central temperature through the vessels in the hairy skin, the interscapular BAT, and the fusimotor fibers to limb muscles, all being silenced by neuronal inhibition of the raphe pallidus and/or magnus (McAllen et al. 2010). Although they all should have a sympathetic premotor relay in these nuclei, these four sympathetic thermoeffector outflows differ in terms of thermal thresholds, relative responsiveness to T_{core}, patterns and driving by neural pathways and thus probably do not "cross talk" at this level (McAllen et al. 2010; Nagashima et al. 2000; Ootsuka and McAllen 2006 ; Romanovsky 2007; Tanaka et al. 2007). The relative contribution of single individual neurons to these functions remains an open question.

Rostrocaudal localization of effective sites. Overall, the injection sites that elicited the most widespread and early latency vasodilation were located in the coronal planes posterior to the interaural line by 1.3–2.6 mm. Eighty-five percent of experiments where the vasodilatation of all areas either on the tail or the paws occurred in <15 min were found in these regions. Again our observations agree with the report by Korsak and Gilbey (2004) showing a similar rostrocaudal extension of their effective sites for blocking by GABA the sympathetic vasoconstrictor drive in the tail. Similarly, brainstem neurons both antidromically activated from the lumbar dorsolateral funiculus and activated by mild cold were found in the raphe nuclei between the coronal planes posterior to the interaural line by 1.8–2.3 mm (Rathner et al. 2001).

Overall, the literature related to thermoregulation points to coronal planes immediately rostral to the rostral pole of the inferior olivary complex at the level of the caudal half of the facial nucleus. This brainstem region is often referred as to the rostral raphe pallidus, although it generally does include the nucleus raphe magnus (e.g., Madden and Morrison 2003, 2005; Morrison 1999, 2003; Morrison et al. 1999, 2000; Rathner et al. 2008). In fact, very few studies were devoted to a systematic mapping.

As pointed out by Nason and Mason (2004), it is unlikely that a microinjection into any single nucleus in RVM/rMR will affect neurons confined to that nucleus because these neurons have large dendritic arbors that cross cytoarchitectonic boundaries (Gao and Mason 1997; Mason et al. 1990; Newman 1985; Potrebic and Mason 1993). Blessing (2003) discussed the conventional anatomical demarcation into RMg and RPa by raising the following points. The delimitation of boundaries is based particularly on the work of Taber et al. (1960) that follows the atlas of Meessen and Olszewski (1949) for rabbits and the atlas of Olszewski and Baxter (1954) for humans. However, the rabbit atlas combines all the ventral midline neurons in the rostral medulla and caudal pons as "RMg" and does not use the term "RPa." In contrast, the human atlas uses "RPa" and not "RMg." However, by convention, RMg in the rat is more rostral and dorsal, and RPa is more caudal and ventral (Paxinos and Watson 1986).

We noted that the HLIs following muscimol microinjection were 20–25% lower than the HLI seen during the maximal physiological vasodilatation achieved in rats maintained in thermoneutral conditions (El Bitar et al. 2014a), suggesting that the ongoing hind paws and tail fiber sympathetic activities were not completly silenced following the microinjections, in spite of a clear ceiling effect when microinjections were effective. The most parsimonious explanation for this observation is the oblong geometry of the involved brainstem structures, ~12 times longer than the diameter of the injected volume, preventing the drug to reach all structures potentially involved in controling vasomotor tone.

In summary, there are morphological and functional reasons to consider the RVM and rMR nuclei as a single RVM/rMR entity, as already proposed by Mason et al. (2001, 2005a,b, 2006, 2011).

Is the RVM really specific for pain/nociception? Our study shows, in the rat, a mutual covering of the regions involved in thermoregulation (at least, regarding the vasomotor tone of the tail and hind paws) with those reported as being specifically involved in pain/nociception.

In spite of several warnings initiated by T. Lovick and P. Mason (Le Bars et al. 2001; Lefler et al. 2008; Lovick 1997; Mason 2001, 2005a,b, 2006, 2011, 2012), the specificity of the RVM regarding the control of pain/nociception mechanisms is repeatedly put forward or assumed (e.g., Fields et al. 2006; Heinricher and Ingram 2008; Basbaum et al. 2009; Heinricher et al. 2009). RVM neurons do not only project towards the dorsal horn of the spinal cord (Fields and Basbaum 1978, 1999), but also to the intermediolateral cell column, with a high degree of collateralization in both the rostrocaudal and dorsoventral axes (Bacon et al. 1990; Basbaum et al. 1978; Hossaini et al. 2012; Lefler et al. 2008; Loewy 1981; Morrison and Gebber 1985).

Numerous neurons in RVM/rMR were identified as sympathetic premotor neurons by early retrograde transsynaptic labeling with the pseudorabies virus (Smith et al. 1998; Strack et al. 1989). Quantitative data, obtained from 6 days survival experiments, revealed approximately five times more labeled neurons in raphe magnus and gigantocellular reticular pars alpha nuclei than within the raphe palidus nucleus (Smith et al. 1998). Smith et al. (1998) found the highest density at the level of the facial nucleus, but the coronal planes facing the rostral part of the facial nucleus were not represented. Therefore, the neurons labeled in that study could have been mainly located in the RVM/rMR at the level of facial nucleus, although we cannot infer their rostral extent. However, it was stated more recently that transneuronally labeled neurons are distributed through the parapyramidal region, including all RVM/rMR elements (Tóth et al. 2006), at least within the coronal planes from 1.3 to 3.3 mm posterior to the interaural line (Nakamura et al. 2004). Finally, cold exposure increases the expression of

Fos immunoreactivity not only in RPa and PPy (Bonaz and Taché 1994; Cano et al. 2003; Martinez et al. 2001; Morrison et al. 1999) but also in RMg, between the coronal planes posterior to the interaural line by 1.3–3.3 mm (Nakamura et al. 2004).

If one moves back to the literature related to nociception, namely the so-called on- and off-cells recorded within the medial brainstem, one is struck by the similar rostrocaudal distribution of the sites, all pointing out the coronal planes including the facial nucleus. Interestingly, Vanegas et al. (1984) attempted to map on- and off-neurons that project to the spinal cord and found that these were located in brain regions 1.9–2.7 mm posterior to the interaural line. In summary, the most effective sites for blocking by muscimol the cutaneous vasoconstrictor fibers matches exactly the brainstem sites where on- and off-cells were recorded over the last years, notably those projecting to the spinal cord.

Pharmacological manipulations of RVM/rMR in pain studies. Administration of muscimol exclusively within RVM/rMR results in a significant decrease in TFL while administration of the competitive $GABA_A$ receptor antagonist bicuculline (but not the glycine receptor antagonist strychnine) induces an increase of the TFL (Drower and Hammond 1988; Gilbert and Franklin 2001; Heinricher and Kaplan 1991; Heinricher and Tortorici 1994; Nason and Mason 2004). Similar results have been reported with paw withdrawal and hot-plate tests (Gilbert and Franklin 2001; Martenson et al. 2009).

These increases or decreases of TFL are generally interpreted in terms of hypo- or hyperalgesia, respectively. However, other interpretations are conceivable, available, and advisable. The tail-flick test does not achieve the criterion of construct validity because it does not effectively measure the targeted construct, i.e., a quantitative nociceptive response, presumed to reflect an animal's perception of pain (Le Bars et al. 2001, 2009). Indeed, the reaction time measured in the conventional tail-flick test (and all other tests using conventional progressive heating) is the sum of *1*) the time to achieve the threshold for the behavioral reaction and *2*) the behavioral latency (Benoist et al. 2008; Pincedé et al. 2012). If the reaction time is the only measured end point, there is no way of knowing whether the variation was produced by changes of either the basal skin temperature or the threshold temperature or both. Using a simple model for computing the TFL in the rat, taking into account the power of the radiant heat source, the initial skin temperature, T_{core}, and the site of stimulation on the tail (Benoist et al. 2008), we predicted that the change in tail temperature 15 min after effective muscimol injection would lead to a 30–35% reduction of the TFL. Interestingly, Heinricher and Kaplan (1991) described a decrease of the TFL of ~30% at 12 min postinjection of muscimol (50 ng; 0.5 μl), maintained throughout the half an hour observation period, a finding reproduced by Meng et al. (1998). Both observations match remarkably the predicted variations of TFL related to changes in baseline skin temperature. Interestingly, Tjølsen and Hole (1997) attributed the reduction of TFL following lesions of the raphe-spinal serotoninergic system to the increase in skin temperature.

It should be noted that such considerations are not restricted to the tests based on the utilization of thermal stimuli. For example, the vasodilatation of the paws induced by high T_{amb} exacerbates the second phase of the formalin test (Rosland 1991; Tjølsen et al. 1992). It follows that the increased responsiveness to formalin injection following muscimol administration in RVM/rMR (Gilbert and Franklin 2001) could also be largely due to the unavoidable vasodilatation.

Conclusion. The functional blockade of the RVM/rMR by muscimol elicits an important increase of skin temperature of the paws and tail, eliciting a reduction of T_{core}. The effective zones match very exactly the brain regions defined as specifically devoted to the control of nociception. Because changes in skin temperature can have a strong effect on the usual tests of pain using radiant heat such as the TFL, our results indicate that the evidence that pharmacological manipulations of RVM/rMR modulate pain-specific descending modulatory pathways could, actually, be explained by unaccounted changes in vasomotor tone.

ACKNOWLEDGMENTS

We thank Pascal Carrive, François Cesselin, and Léon Plaghki for advice in the preparation of the manuscript.

GRANTS

N. El Bitar was supported by a grant from the Société Française d'Etude et de Traitement de la Douleur (SFETD) et l'Institut UPSA de la Douleur (IUD).

DISCLOSURES

No conflicts of interest, financial or otherwise, are declared by the author(s).

AUTHOR CONTRIBUTIONS

Author contributions: N.E.B., B.P., and D.L.B. conception and design of research; N.E.B., B.P., and D.L.B. performed experiments; N.E.B., B.P., G.H., A.M., and D.L.B. analyzed data; N.E.B. and D.L.B. interpreted results of experiments; N.E.B., B.P., A.M., and D.L.B. drafted manuscript; N.E.B., A.M., and D.L.B. edited and revised manuscript; N.E.B., A.M., and D.L.B. approved final version of manuscript; A.M. and D.L.B. prepared figures.

REFERENCES

Allen TA, Narayanan NS, Kholodar-Smith DB, Zhao Y, Laubach M, Brown TH. Imaging the spread of reversible brain inactivations using fluorescent muscimol. *J Neurosci Methods* 171: 30–38, 2008.

Bacon SJ, Zagon A, Smith AD. Electron microscopic evidence of a monosynaptic pathway between cells in the caudal raphe nuclei and sympathetic preganglionic neurons in the rat spinal cord. *Exp Brain Res* 79: 589–602, 1990.

Barbaro NM, Heinricher MM, Fields HL. Putative nociceptive modulatory neurons in the rostral ventromedial medulla of the rat display highly correlated firing patterns. *Somatosens Mot Res* 6: 413–425, 1989.

Basbaum AI, Fields HL. The origin of descending pathways in the dorsolateral funiculus of the spinal cord of the cat and rat: further studies on the anatomy of pain modulation. *J Comp Neurol* 187: 513–531, 1979.

Basbaum AI, Clanton CH, Fields HL. Three bulbospinal pathways from the rostral medulla of the cat: an autoradiographic study of pain modulating systems. *J Comp Neurol* 178: 209–224, 1978.

Basbaum AI, Braz J, Ossipov MH, Porreca F. The endogenous neuromodulation system. In: *Neuromodulation*, edited by Krames E, Peckham PH, Rezai A. London: Academic, 2009, p. 303–312.

Beaumont K, Chilton WS, Yamamura HI, Enna SJ. Muscimol binding in rat brain: association with synaptic GABA receptors. *Brain Res* 148: 153–162, 1978.

Benoist JM, Pincedé I, Ballantyne K, Plaghki L, Le Bars D. Peripheral and central determinants of a nociceptive reaction: an approach to psychophysics in the rat. *PLoS One* 3: e3125, 2008.

Bernard JF, Netzer F, Gau R, Hamon M, Laguzzi R, Sévoz-Couche C. Critical role of B3 serotonergic cells in baroreflex inhibition during the defense reaction triggered by dorsal periaqueductal gray stimulation. *J Comp Neurol* 506: 108–121, 2008.

Blessing WW. Lower brainstem pathways regulating sympathetically mediated changes in cutaneous blood flow. *Cell Mol Neurobiol* 23: 527–538, 2003.

Blessing WW, Nalivaiko E. Cutaneous vascular bed is not involved in arterial pressure changes elicited by increasing or decreasing the activity of inhibitory vasomotor neurons in caudal ventrolateral medulla in rabbits. *Neurosci Lett* 290: 141–144, 2000.

Blessing WW, Nalivaiko E. Raphe magnus/pallidus neurons regulate tail but not mesenteric arterial blood flow in rats. *Neuroscience* 105: 923–929, 2001.

Blessing WW, Yu YH, Nalivaiko E. Raphe pallidus and parapyramidal neurons regulate ear pinna vascular conductance in the rabbit. *Neurosci Lett* 270: 33–36, 1999.

Bonaz B, Taché Y. Induction of Fos immunoreactivity in the rat brain after cold-restraint induced gastric lesions and fecal excretion. *Brain Res* 652: 56–64, 1994.

Bondareff W, Routtenberg A, Narotzky R, McLone DG. Intrastriatal spreading of biogenic amines. *Exp Neurol* 28: 213–229, 1970.

Brink TS, Hellman KM, Lambert AM, Mason P. Raphe magnus neurons help protect reactions to visceral pain from interruption by cutaneous pain. *J Neurophysiol* 96: 3423–3432, 2006.

Cano G, Passerin AM, Schiltz JC, Card JP, Morrison SF, Sved AF. Anatomical substrates for the central control of sympathetic outflow to interscapular adipose tissue during cold exposure. *J Comp Neurol* 460: 303–326, 2003.

Cao WH, Morrison SF. Disinhibition of rostral raphe pallidus neurons increases cardiac sympathetic nerve activity and heart rate. *Brain Res* 980: 1–10, 2003.

Cao WH, Fan W, Morrison SF. Medullary pathways mediating specific sympathetic responses to activation of dorsomedial hypothalamus. *Neuroscience* 126: 229–240, 2004.

Cao WH, Madden CJ, Morrison SF. Inhibition of brown adipose tissue thermogenesis by neurons in the ventrolateral medulla and in the nucleus tractus solitarius. *Am J Physiol Regul Integr Comp Physiol* 299: R277–R290, 2010.

Carlson JD, Maire JJ, Martenson ME, Heinricher MM. Sensitization of pain-modulating neurons in the rostral ventromedial medulla after peripheral nerve injury. *J Neurosci* 27: 13222–13231, 2007.

Carrive P, Churyukanov M, Le Bars D. A reassessment of stress-induced "analgesia" in the rat using an unbiased method. *Pain* 152: 676–686, 2011.

Cerri M, Zamboni G, Tupone D, Dentico D, Luppi M, Martelli D, Perez E, Amici R. Cutaneous vasodilation elicited by disinhibition of the caudal portion of the rostral ventromedial medulla of the free-behaving rat. *Neuroscience* 165: 984–995, 2010.

Covino BG, Dubner R, Gybels J, Kosterlitz HW, Liebeskind JC, Sternbach RA, Vycklický L, Yamamura H, Zimmermann M. Ethical standards for investigations of experimental pain in animals. The Committee for Research and Ethical Issues of the International Association for the Study of Pain. *Pain* 9: 141–143, 1980.

Drower EJ, Hammond DL. GABAergic modulation of nociceptive threshold: effects of THIP and bicuculline microinjected in the ventral medulla of the rat. *Brain Res* 450: 316–324, 1988.

Edeline JM, Hars B, Hennevin E, Cotillon N. Muscimol diffusion after intracerebral microinjections: a reevaluation based on electrophysiological and autoradiographic quantifications. *Neurobiol Learn Mem* 78: 100–124, 2002.

El Bitar N, Pollin B, Karroum EG, Pincedé I, Mouraux A, Le Bars D. Thermoregulatory vasomotor tone of the rat tail and paws in thermoneutral conditions and its impact on a behavioral model of acute pain. *J Neurophysiol* 112: 2185–2198, 2014a.

El Bitar N, Pollin B, Le Bars D. "On-" and "off-" cells in the rostral ventromedial medulla of rats held in thermoneutral conditions: are they involved in thermoregulation? *J Neurophysiol* 112: 2199–2217, 2014b.

Enna SJ, Snyder SH. Properties of gamma-aminobutyric acid (GABA) receptor binding in rat brain synaptic membrane fractions. *Brain Res* 100: 81–97, 1975.

Fan W, Morrison SF, Cao WH, Yu P. Thermogenesis activated by central melanocortin signaling is dependent on neurons in the rostral raphe pallidus (rRPa) area. *Brain Res* 1179: 61–69, 2007.

Fields HL, Basbaum AI. Brainstem control of spinal pain-transmission neurons. *Annu Rev Physiol* 40: 217–248, 1978.

Fields HL, Basbaum AI. Central nervous system mechanisms of pain modulation. In: *Textbook of Pain*, edited by Wall PD, Melzack R. London: Churchill Livingstone, 1999, p. 309–329.

Fields HL, Bry J, Hentall I, Zorman G. The activity of neurons in the rostral medulla of the rat during withdrawal from noxious heat. *J Neurosci* 3: 2545–2552, 1983.

Fields HL, Malick A, Burstein R. Dorsal horn projection targets of ON and OFF cells in the rostral ventromedial medulla. *J Neurophysiol* 74: 1742–1759, 1995.

Fields HL, Basbaum AI, Heinricher MM. Central nervous system mechanisms of pain modulation. In: *Wall and Melzack's Textbook of Pain*, edited by McMahon SB, Koltzenburg M. Edinburgh, Scotland: Elsevier Churchill Livingstone, 2006, p. 125–142.

Gallagher JP, Nakamura J, Shinnick-Gallagher P. Effects of glial uptake and desensitization on the activity of gamma-aminobutyric acid (GABA) and its analogs at the cat dorsal root ganglion. *J Pharmacol Exp Ther* 226: 876–884, 1983.

Gao K, Mason P. Somatodendritic and axonal anatomy of intracellularly labeled serotonergic neurons in the rat medulla. *J Comp Neurol* 389: 309–328, 1997.

Gilbert AK, Franklin KB. GABAergic modulation of descending inhibitory systems from the rostral ventromedial medulla (RVM). Dose-response analysis of nociception and neurological deficits. *Pain* 90: 25–36, 2001.

Gordon CJ, Puckett E, Padnos B. Rat tail skin temperature monitored noninvasively by radiotelemetry: characterization by examination of vasomotor responses to thermomodulatory agents. *J Pharmacol Toxicol Methods* 47: 107–114, 2002.

Heinricher MM, Ingram SL. The brainstem and nociceptive modulation. In: *The Senses: a Comprehensive Reference*, edited by Basbaum AI, Akimichi K, Gordon MS, Westheimer G. Waltham, MA: Elsevier Academic, 2008, p. 593–626.

Heinricher MM, Kaplan HJ. GABA-mediated inhibition in rostral ventromedial medulla: role in nociceptive modulation in the lightly anesthetized rat. *Pain* 47: 105–113, 1991.

Heinricher MM, Tortorici V. Interference with GABA transmission in the rostral ventromedial medulla: disinhibition of off-cells as a central mechanism in nociceptive modulation. *Neuroscience* 63: 533–546, 1994.

Heinricher MM, Tavares I, Leith JL, Lumb BM. Descending control of nociception: specificity, recruitment and plasticity. *Brain Res Rev* 60: 214–225, 2009.

Helke CJ, Thor KB, Sasek CA. Chemical neuroanatomy of the parapyramidal region of the ventral medulla in the rat. *Prog Brain Res* 81: 17–28, 1989.

Hertzman AB. Some relations between skin temperature and blood flow. *Am J Phys Med* 32: 233–251, 1953.

Hikosaka O, Wurtz RH. Modification of saccadic eye movements by GABA-related substances. I. Effect of muscimol and bicuculline in monkey superior colliculus. *J Neurophysiol* 53: 266–291, 1985.

Hossaini M, Goos JA, Kohli SK, Holstege JC. Distribution of glycine/GABA neurons in the ventromedial medulla with descending spinal projections and evidence for an ascending glycine/GABA projection. *PLoS One* 7: e35293, 2012.

Kaplan H, Fields HL. Hyperalgesia during acute opioid abstinence: evidence for a nociceptive facilitating function of the rostral ventromedial medulla. *J Neurosci* 11: 1433–1439, 1991.

Knoppers AT. La queue du rat, témoin de la régulation thermique. *Arch Néer Physiol* 26: 364–406, 1942.

Korsak A, Gilbey MP. Rostral ventromedial medulla and the control of cutaneous vasoconstrictor activity following icv prostaglandin E_1. *Neuroscience* 124: 709–717, 2004.

Krogsgaard-Larsen P, Johnston GA, Lodge D, Curtis DR. A new class of GABA agonist. *Nature* 268: 53–55, 1977.

Le Bars D, Gozariu M, Cadden SW. Animal models of nociception. *Pharmacol Rev* 53: 597–652, 2001.

Le Bars D, Hansson P, Plaghki L. Current animal test and models of pain. In: *Pharmacology of Pain*, edited by Beaulieu P, Lussier D, Porreca F, Dickenson AH. Seattle, WA: IASP, 2009, p. 475–504.

Lefler Y, Arzi A, Reiner K, Sukhotinsky I, Devor M. Bulbospinal neurons of the rat rostromedial medulla are highly collateralized. *J Comp Neurol* 506: 960–978, 2008.

Light AR. The spinal terminations of single, physiologically characterized axons originating in the pontomedullary raphe of the cat. *J Comp Neurol* 234: 536–548, 1985.

Lin MT, Chern YF, Liu GG, Chang TC. Studies on thermoregulation in the rat. *Proc Natl Sci Council ROC* 3: 46–52, 1979.

Loewy AD. Raphe pallidus and raphe obscurus projections to the intermediolateral cell column in the rat. *Brain Res* 222: 129–133, 1981.

Lovick TA. The medullary raphe nuclei: a system for integration and gain control in autonomic and somatomotor responsiveness? *Exp Physiol* 82: 31–41, 1997.

Lynn RB, Kreider MS, Miselis RR. Thyrotropin-releasing hormone-immunoreactive projections to the dorsal motor nucleus and the nucleus of the solitary tract of the rat. *J Comp Neurol* 311: 271–288, 1991.

Madden CJ, Morrison SF. Excitatory amino acid receptor activation in the raphe pallidus area mediates prostaglandin-evoked thermogenesis. *Neuroscience* 122: 5–15, 2003.

Madden CJ, Morrison SF. Hypoxic activation of arterial chemoreceptors inhibits sympathetic outflow to brown adipose tissue in rats. *J Physiol* 566: 559–573, 2005.

Malpeli JG. Reversible inactivation of subcortical sites by drug injection. *J Neurosci Methods* 86: 119–128, 1999.

Martenson ME, Cetas JS, Heinricher MM. A possible neural basis for stress-induced hyperalgesia. *Pain* 142: 236–244, 2009.

Martin JH. Autoradiographic estimation of the extent of reversible inactivation produced by microinjection of lidocaine and muscimol in the rat. *Neurosci Lett* 127: 160–164, 1991.

Martin JH, Ghez C. Pharmacological inactivation in the analysis of the central control of movement. *J Neurosci Methods* 86: 145–159, 1999.

Martínez V, Wang L, Taché Y. Central TRH receptor 1 antisense blocks cold-induced gastric emptying but not brain c-Fos induction. *Peptides* 22: 81–90, 2001.

Mason P. Contributions of the medullary raphe and ventromedial reticular region to pain modulation and other homeostatic functions. *Annu Rev Neurosci* 24: 737–777, 2001.

Mason P. Deconstructing endogenous pain modulations. *J Neurophysiol* 94: 1659–1663, 2005a.

Mason P. Ventromedial medulla: pain modulation and beyond. *J Comp Neurol* 493: 2–8, 2005b.

Mason P. Descending pain modulation as a component of homeostasis. In: *Pain*, edited by Cervero F, Jensen TS. Waltham, MA: Elsevier, 2006, p. 211–218.

Mason P. From descending pain modulation to obesity via the medullary raphe. *Pain* 152: S20–S24, 2011.

Mason P. Medullary circuits for nociceptive modulation. *Curr Opin Neurobiol* 22: 640–645, 2012.

Mason P, Floeter MK, Fields HL. Somatodendritic morphology of on- and off-cells in the rostral ventromedial medulla. *J Comp Neurol* 301: 23–43, 1990.

McAllen RM, Tanaka M, Ootsuka Y, McKinley MJ. Multiple thermoregulatory effectors with independent central controls. *Eur J Appl Physiol* 109: 27–33, 2010.

Meessen H, Olszewski J. *A Cytoarchitectonic Atlas of the Rhombencephalon of the Rabbit*. Basel, Switzerland: Karger, 1949.

Meng ID, Manning BH, Martin WJ, Fields HL. An analgesia circuit activated by cannabinoids. *Nature* 395: 381–383, 1998.

Morgan MM, Fields HL. Pronounced changes in the activity of nociceptive modulatory neurons in the rostral ventromedial medulla in response to prolonged thermal noxious stimuli. *J Neurophysiol* 72: 1161–1170, 1994.

Morrison SF. RVLM and raphe differentially regulate sympathetic outflows to splanchnic and brown adipose tissue. *Am J Physiol Regul Integr Comp Physiol* 276: R962–R973, 1999.

Morrison SF. Differential regulation of brown adipose and splanchnic sympathetic outflows in rat: roles of raphe and rostral ventrolateral medulla neurons. *Clin Exp Pharmacol Physiol* 28: 138–143, 2001.

Morrison SF. Raphe pallidus neurons mediate prostaglandin E2-evoked increases in brown adipose tissue thermogenesis. *Neuroscience* 121: 17–24, 2003.

Morrison SF. Activation of 5-HT1A receptors in raphe pallidus inhibits leptin-evoked increases in brown adipose tissue thermogenesis. *Am J Physiol Regul Integr Comp Physiol* 286: R832–R837, 2004.

Morrison SF. 2010 Carl Ludwig Distinguished Lectureship of the APS Neural Control and Autonomic Regulation Section: Central neural pathways for thermoregulatory cold defense. *J Appl Physiol* 110: 1137–1149, 2011.

Morrison SF, Gebber GL. Axonal branching patterns and funicular trajectories of raphespinal sympathoinhibitory neurons. *J Neurophysiol* 53: 759–772, 1985.

Morrison SF, Sved AF, Passerin AM. GABA-mediated inhibition of raphe pallidus neurons regulates sympathetic outflow to brown adipose tissue. *Am J Physiol Regul Integr Comp Physiol* 276: R290–R297, 1999.

Morrison SF, Ramamurthy S, Young JB. Reduced rearing temperature augments responses in sympathetic outflow to brown adipose tissue. *J Neurosci* 20: 9264–9271, 2000.

Morrison SF, Nakamura K, Madden CJ. Central control of thermogenesis in mammals. *Exp Physiol* 93: 773–797, 2008.

Morrison SF, Madden CJ, Tupone D. Central control of brown adipose tissue thermogenesis. *Front Endocrinol (Lausanne)* 3: 1–19, 2012.

Myers RD. Injection of solutions into cerebraltissue: relation between volume and diffusion. *Physiol Behav* 1: 171–174, 1966.

Nagashima K, Nakai S, Tanaka M, Kanosue K. Neuronal circuitries involved in thermoregulation. *Auton Neurosci* 85: 18–25, 2000.

Nakamura K. Central circuitries for body temperature regulation and fever. *Am J Physiol Regul Integr Comp Physiol* 301: R1207–R1228, 2011.

Nakamura K, Morrison SF. Central efferent pathways mediating skin cooling-evoked sympathetic thermogenesis in brown adipose tissue. *Am J Physiol Regul Integr Comp Physiol* 292: R127–R136, 2007.

Nakamura K, Morrison SF. A thermosensory pathway that controls body temperature. *Nat Neurosci* 11: 62–71, 2008.

Nakamura K, Morrison SF. Central efferent pathways for cold-defensive and febrile shivering. *J Physiol* 589: 3641–3658, 2011.

Nakamura K, Matsumura K, Hubschle T, Nakamura Y, Hioki H, Fujiyama F, Boldogköi Z, Konig M, Thiel HJ, Gerstberger R, Kobayashi S, Kaneko T. Identification of sympathetic premotor neurons in medullary raphe regions mediating fever and other thermoregulatory functions. *J Neurosci* 24: 5370–5380, 2004.

Nason MW Jr, Mason P. Modulation of sympathetic and somatomotor function by the ventromedial medulla. *J Neurophysiol* 92: 510–522, 2004.

Neubert MJ, Kincaid W, Heinricher MM. Nociceptive facilitating neurons in the rostral ventromedial medulla. *Pain* 110: 158–165, 2004.

Newman DB. Distinguishing rat brainstem reticulospinal nuclei by their neuronal morphology. I. Medullary nuclei. *J Hirnforsch* 26: 187–226, 1985.

Nicholson SH, Suckling CJ, Iversen LL. GABA analogues: conformational analysis of effects on [3H]GABA binding to postsynaptic receptors in human cerebellum. *J Neurochem* 32: 249–252, 1979.

Olszewski J, Baxter D. *Cytoarchitecture of the Human Brain Stem*. Basel, Switzerland: Karger, 1954.

Ootsuka Y, McAllen RM. Interactive drives from two brain stem premotor nuclei are essential to support rat tail sympathetic activity. *Am J Physiol Regul Integr Comp Physiol* 289: R1107–R1115, 2005.

Ootsuka Y, McAllen RM. Comparison between two rat sympathetic pathways activated in cold defense. *Am J Physiol Regul Integr Comp Physiol* 291: R589–R595, 2006.

Ootsuka Y, Blessing WW, McAllen RM. Inhibition of rostral medullary raphé neurons prevents cold-induced activity in sympathetic nerves to rat tail and rabbit ear arteries. *Neurosci Lett* 357: 58–62, 2004.

Paxinos G, Watson C. *The Rat Brain in Stereotaxic Coordinates*. Sydney, Australia: Academic, 1986.

Pincedé I, Pollin B, Meert T, Plaghki L, Le Bars D. Psychophysics of a nociceptive test in the mouse. *PLoS One* 7: e36699, 2012.

Potrebic SB, Mason P. Three-dimensional analysis of the dendritic domains of on- and off-cells in the rostral ventromedial medulla. *J Comp Neurol* 337: 83–93, 1993.

Rathner JA, McAllen RM. Differential control of sympathetic drive to the rat tail artery and kidney by medullary premotor cell groups. *Brain Res* 834: 196–199, 1999.

Rathner JA, Owens NC, McAllen RM. Cold-activated raphe-spinal neurons in rats. *J Physiol* 535: 841–854, 2001.

Rathner JA, Madden CJ, Morrison SF. Central pathway for spontaneous and prostaglandin E_2-evoked cutaneous vasoconstriction. *Am J Physiol Regul Integr Comp Physiol* 295: R343–R354, 2008.

Romanovsky AA. Thermoregulation: some concepts have changed. Functional architecture of the thermoregulatory system. *Am J Physiol Regul Integr Comp Physiol* 292: R37–R46, 2007.

Romanovsky AA, Ivanov AI, Shimansky YP. Selected contribution: ambient temperature for experiments in rats: a new method for determining the zone of thermal neutrality. *J Appl Physiol* 92: 2667–2679, 2002.

Rosland JH. The formalin test in mice: the influence of ambient temperature. *Pain* 45: 211–216, 1991.

Salo LM, Nalivaiko E, Anderson CR, McAllen RM. Control of cardiac rate, contractility, and atrioventricular conduction by medullary raphe neurons in anesthetized rats. *Am J Physiol Heart Circ Physiol* 296: H318–H324, 2009.

Smith JE, Jansen AS, Gilbey MP, Loewy AD. CNS cell groups projecting to sympathetic outflow of tail artery: neural circuits involved in heat loss in the rat. *Brain Res* 786: 153–164, 1998.

Strack AM, Sawyer WB, Hughes JH, Platt KB, Loewy AD. A general pattern of CNS innervation of the sympathetic outflow demonstrated by transneuronal pseudorabies viral infections. *Brain Res* 491: 156–162, 1989.

Syková E, Nicholson C. Diffusion in brain extracellular space. *Physiol Rev* 88: 1277–1340, 2008.

Székely M. Skin temperature-skin blood flow: assessment of thermoregulatory changes. *Acta Physiol Hung* 68: 284, 1986.

Taber E, Brodal A, Walberg F. The raphe nuclei of the brain stem in the cat. I. Normal topography and cytoarchitecture and general discussion. *J Comp Neurol* 114: 161–187, 1960.

Tanaka M, Nagashima K, McAllen RM, Kanosue K. Role of the medullary raphe in thermoregulatory vasomotor control in rats. *J Physiol* 540: 657–664, 2002.

Tanaka M, Ootsuka Y, McKinley MJ, McAllen RM. Independent vasomotor control of rat tail and proximal hairy skin. *J Physiol* 582: 421–433, 2007.

Thorington RW Jr. *The Biology of Rodent Tails: A Study of Form and Function* (PhD thesis). Fort Wainwright, AL: Arctic Aeromedical Laboratory, 1966.

Thurston CL, Helton ES. Effects of intravenous phenylephrine on blood pressure, nociception, and neural activity in the rostral ventral medulla in rats. *Brain Res* 717: 81–90, 1996.

Thurston CL, Randich A. Effects of vagal afferent stimulation on ON and OFF cells in the rostroventral medulla: relationships to nociception and arterial blood pressure. *J Neurophysiol* 67: 180–196, 1992.

Thurston CL, Randich A. Responses of on and off cells in the rostral ventral medulla to stimulation of vagal afferents and changes in mean arterial blood pressure in intact and cardiopulmonary deafferented rats. *Pain* 62: 19–38, 1995.

Tjølsen A, Hole K. Animal models of analgesia. In: *Pharmacology of Pain*, edited by Dickenson AH, Besson JM. Berlin, Germany: Springer, 1997, p. 1–20.

Tjølsen A, Berge OG, Hunskaar S, Rosland JH, Hole K. The formalin test: an evaluation of the method. *Pain* 51: 5–17, 1992.

Tóth IE, Tóth DE, Boldogkoi Z, Hornyák A, Palkovits M, Blessing WW. Serotonin-synthesizing neurons in the rostral medullary raphé/parapyramidal region transneuronally labelled after injection of pseudorabies virus into the rat tail. *Neurochem Res* 31: 277–286, 2006.

Vanegas H, Barbaro NM, Fields HL. Tail-flick related activity in medullospinal neurons. *Brain Res* 321: 135–141, 1984.

Vianna DM, Allen C, Carrive P. Cardiovascular and behavioral responses to conditioned fear after medullary raphe neuronal blockade. *Neuroscience* 153: 1344–1353, 2008.

Wu Y, Jiji LM, Lemons DE, Weinbaum S. A non-uniform three-dimensional perfusion model of rat tail heat transfer. *Phys Med Biol* 40: 789–806, 1995.

Xu M, Kim CJ, Neubert MJ, Heinricher MM. NMDA receptor-mediated activation of medullary pro-nociceptive neurons is required for secondary thermal hyperalgesia. *Pain* 127: 253–262, 2007.

Yoshida K, Nakamura K, Matsumura K, Kanosue K, König M, Thiel HJ, Boldogköi Z, Toth I, Roth J, Gerstberger R, Hübschle T. Neurons of the rat preoptic area and the raphe pallidus nucleus innervating the brown adipose tissue express the prostaglandin E receptor subtype EP3. *Eur J Neurosci* 18: 1848–1860, 2003.

Young AA, Dawson NJ. Evidence for on-off control of heat dissipation from the tail of the rat. *Can J Physiol Pharmacol* 60: 392–398, 1982.

Zaretsky DV, Zaretskaia MV, DiMicco JA. Stimulation and blockade of GABA(A) receptors in the raphe pallidus: effects on body temperature, heart rate, and blood pressure in conscious rats. *Am J Physiol Regul Integr Comp Physiol* 285: R110–R116, 2003a.

Zaretsky DV, Zaretskaia MV, Samuels BC, Cluxton LK, DiMicco JA. Microinjection of muscimol into raphe pallidus suppresses tachycardia associated with air stress in conscious rats. *J Physiol* 546: 243–250, 2003b.

Zimmermann M. Ethical guidelines for investigations of experimental pain in conscious animals. *Pain* 16: 109–110, 1983.